Author/s:
Liu, X;Zeng, P;Chen, S;Smith, TA;Liu, M

Title:
Charge Transfer Dynamics at the Interface of CsPbX Perovskite Nanocrystal-Acceptor Complexes: A Femtosecond Transient Absorption Spectroscopy Study

Date:
2022-12

Citation:
Liu, X., Zeng, P., Chen, S., Smith, T. A. & Liu, M. (2022). Charge Transfer Dynamics at the Interface of CsPbX Perovskite Nanocrystal-Acceptor Complexes: A Femtosecond Transient Absorption Spectroscopy Study. Laser and Photonics Reviews, 16 (12), https://doi.org/10.1002/lpor.202200280.

Persistent Link:
https://hdl.handle.net/11343/332235

Charge Transfer Dynamics at the Interface of $CsPbX_3$ Perovskite Nanocrystal-Acceptor Complexes: a Femtosecond Transient Absorption Spectroscopy Study

*Xiaochun Liu,[#] Peng Zeng,[#] Shuhan Chen, Trevor A. Smith, and Mingzhen Liu**

Dr. X. Liu, Dr. P. Zeng, S. Chen and Prof. M. Liu

School of Materials and Energy, University of Electronic Science and Technology of China, Chengdu 611731, P.R. China.

E-mail: mingzhen.liu@uestc.edu.cn

Prof. T. A. Smith

ARC Centre of Excellence in Exciton Science & School of Chemistry, The University of Melbourn, Parkville 3010, Victoria, Australia.

Keywords: $CsPbX_3$ perovskite nanocrystal, charge transfer, femtosecond transient absorption spectroscopy, multiple charge transfer pathway effect, surface ligand effect, hot carrier transfer

[#] X.L. and P.Z. contributed equally to this work.

$CsPbX_3$ ($X=I^-$, Br^-, Cl^-) perovskite nanocrystals (PeNCs) are being explored extensively due to their impressive optoelectronic and photonic properties. Efficient harvest of photogenerated charge carriers from the particle is essential for photon-to-current conversion and enhancement of the performance of PeNC-based photovoltaic and optoelectronic

applications. Since photoinduced charge transfer (CT) from the particle usually occurs on sub-picosecond to nanosecond timescales, time-resolved transient absorption (TA) spectroscopy is a powerful technique to investigate this transient dynamic photo-induced process. Herein we review reported investigations, primarily employing femtosecond TA spectroscopy, of the CT process in $CsPbX_3$ PeNCs. Based on the interpretation of TA spectral features and the basic model of CT dynamics, we address the concerns of CT rates or efficiency characterization in TA measurements, including multiple CT pathway effects, surface ligand effects and hot charge carrier extraction. We also provide an elucidation of plasmon-induced hot electron transfer in $CsPbX_3$ PeNC-noble metal heterostructures for their promising potential to contribute the development of $CsPbX_3$ PeNC-based hot carrier devices. We hope that this review can provide deeper insights into the photovoltaic conversion in order to make the most of the CT process in $CsPbX_3$ PeNCs.

1. Introduction

Owing to the triumph of perovskite photovoltaics, the emergence of all inorganic $CsPbX_3$ ($X=I^-$, Br^-, Cl^-) perovskite nanocrystals (PeNCs) has attracted significant interest since the first successes in their synthesis.[1-3] These substances inherit merits of being excellent optoelectronic and photonic materials from bulk perovskites, while combining unique properties of nano-sized structures that enable more size-tunable properties.[4-8] $CsPbX_3$ PeNCs in particular, stand out among the diverse perovskite family for their high stability relative to most organic-inorganic hybrid series.

PeNCs have already become a promising alternative to conventional semiconductor nanostructures. Much effort has been concentrated on synthesis chemistry[9-11] of PeNCs and their device fabrications.[12-15] For most optoelectronic applications, the charge transfer (CT) process plays a deterministic role which sets an intrinsic limit for device performance. In a typical scenario, the photoexcitation promotes an electron to an excited state described by a wavefunction that is delocalized through the nanoparticle. A hole results and a bound electron-hole pair, also often termed an exciton, is subsequently formed. The complete electron/hole extraction from the particle to any outer acceptors can account for the photon-to-current conversion. In order to realize high-performance optoelectronic devices, it is necessary to make the most of the CT process.

The underlying mechanisms of the CT process in $CsPbX_3$ PeNCs are still being unraveled. Intensive efforts are forging links between fundamental discoveries regarding the mechanism and practical applications for these novel nanostructures.[16-19] The very basic issue is the measurement or characterization of the rates or efficiency of the CT process, which is the main focus of this Review. Commonly the CT occurs on a timescale ranging from femtoseconds to hundreds of nanoseconds. Ultrafast laser spectroscopy techniques, especially femtosecond transient absorption (TA) spectroscopy, have been widely recognized as powerful tools to provide straightforward insights into the CT process in the PeNCs. However, there still remain concerns that need to be clarified. In this Review, we first present a fundamental interpretation of TA spectral features and move on to the model of CT dynamics. Then we address the concerns particularly relating to the TA measurements of CT time constants or rates in $CsPbX_3$ PeNCs from the following aspects: 1) Multiple CT pathway

effects; 2) Surface ligand effects on the CT process; and 3) Hot charge carrier extraction. We hope this Review helps to clarify concerns on ultrafast spectroscopy and provides a perspective guidance to measurements of CT processes.

2. Interpretation of TA spectral features

The basic idea of TA spectroscopy is to track changes in the optical density (OD) spectra of samples, along with delay time after pulsed excitation[20, 21] based on the well-known pump-probe technique. For most PeNCs, the ΔOD spectra are often a superposition of three types of signals namely ground state bleach (GSB), stimulated emission (SE), and photo-induced absorption (PIA).[18, 22] In general the GSB is spectrally accompanied by PIAs. **Figure 1a** shows a typical transient absorption spectra of $CsPbBr_3$ PeNCs after excitation at high photo energy above the bandgap. Two types of PIA features are observed in the case for $CsPbBr_3$ PeNCs, on either side of the GSB signal and differ in their lifespan.[23] The GSB signal is commonly induced by the population of corresponding state energy levels after photo-excitation. The population process usually reduces the ability to absorb photons from the ground state with corresponding energies mainly due to the band filling effects. As a result, the peak position of the GSB signal matches with the first excitonic absorption peak. Nevertheless, Kamat et al.[24] observed a charge density-dependent blueshift of the GSB signal. They explained the change of optical bandgap on the basis of Burstein-Moss effect. In detail, as the pump fluence increases, charge carriers are accumulated at band-edge states and thus enable higher-energy optical transitions as illustrated in Figure 1b, leading to a blue shit in the transient GSB feature.

The PIA signals are more often generated by the population of excited energy levels which enables photon absorption from the excited state. The short-lived sub-bandgap PIA signal (PIA2 in Figure 1a) has been verified in association with the bandgap renormalization effect is the exact trigger.[22] Immediately on photoexcitation, a temporary boost of free carriers can induce bandgap renormalization, which leads to new unoccupied states at energies slightly below the bandedge thus a rise in the subgap optical transitions. Within a sub-ps timescale, the PIA2 is soon overwhelmed by the GSB signal as the unoccupied states are refilled by the relaxed hot carriers. Some other works hold the opinion that polarons formed from pump-excitons may contribute to the short-lived PIA2 signal.[25, 26]

As for the long-lived PIA signal (PIA1) above the bandgap, it was previously ascribed to the induced absorption arising from the lowest excitonic state.[18] Afterward, it was evidenced to represent a parity-forbidden exciton transition by careful TA spectroscopic examinations.[27] However, in weakly-confined PeNCs, the spectral feature is much less distinct in comparison to the strongly confinement. The latter exerts large symmetry-breaking perturbation on excitons confined in the same space where the polarons form, and thus give rise to more obvious above bandgap PIA signal (Figure 1c).

Besides, the early-stage TA spectra, which is composed of the GSB and PIA features, seem like the second derivative of steady-state absorption spectra (Figure 1d). From the possible many-body exciton interaction effect, the derivative-like spectral features are attributed to the well-known multi-exciton effect, which arises from the Coulomb interaction between the hot

excitons and band-edge excitons.[28, 29] Meanwhile, multi-exciton effect also gives rise to a gradual spectral redshift in early stage and this behavior is also known as Stark effect.

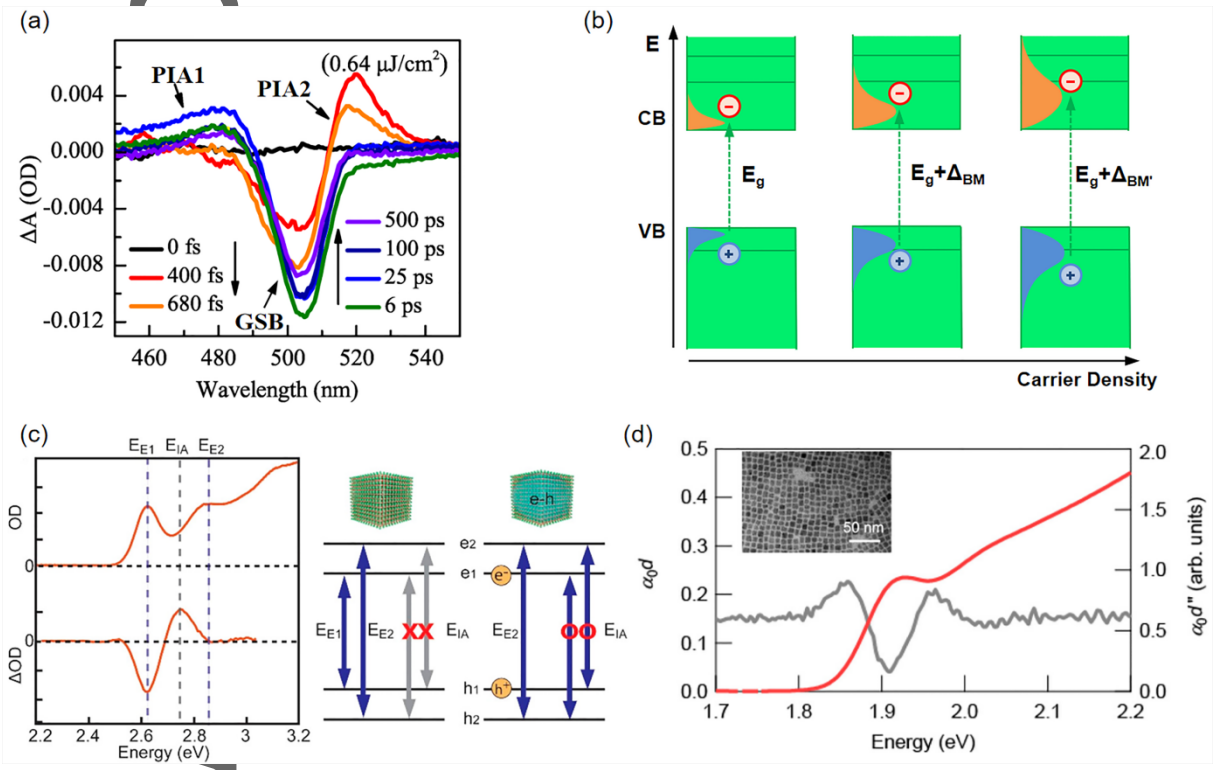

Figure 1. (a) TA spectra of $CsPbBr_3$ NCs at the indicated delay time after excitation at 375 nm. Adapted with permission.[23] Copyright 2021, MDPI. (b) Schematic illustration of the Burstein-Moss effect. VB and CB, the valance band and conduction band of semiconductors (c) Left: ground- and excited-state absorption spectra of $CsPbBr_3$ PeNCs with the size of 4.1 nm; Right: schematic diagram of light-induced activation of forbidden transition in strong quantum confined $CsPbBr_3$ PeNCs. E_{E1} and E_{E2} are the energies of the first and second exciton transitions. E_{IA}, the induce absorption. e_1, e_2, h_1, and h_2 represent electron and hole levels of $CsPbBr_3$ PeNCs. Reproduced with permission.[27] Copyright 2018, American Chemical Society. (d) Absorption spectrum (red curve on the left axis) and the second derivative of the absorption spectrum (gray curve on the right axis) of the $CsPbI_3$ PeNCs. Reproduced with permission.[29] Copyright 2018, American Chemical Society.

Generally, the induced hot excitons/carriers undergo a fast (fs) relaxation process to the band-edge states, whereas the CT occurs on picosecond (ps) or even longer timescales.

Therefore, most CT is from the excited electrons or holes at band-edge levels. In addition, we will also later discuss some hot CT process.

It is worth noting that, unlike conventional II-IV quantum dots (QDs), in which the GSB is dominated by electrons, $CsPbX_3$ PeNCs show the GSB is contributed by both the electron and hole, as a result of the similar effective masses of both.[30, 31] In particular, for an ensemble of nanoparticles, the GSB signal, ΔOD, can be modeled using the average number of photoinduced *e-h* pairs per particle, $\langle N \rangle$, under the assumption of the Poisson distribution considering a simple 2-degeneracy energy level system:[32]

$$\Delta OD/OD = 1 - [1 + \langle N \rangle/2]\exp(-\langle N \rangle) \qquad (1)$$

In a weak excitation mode where $\langle N \rangle \ll 1$, one may make the approximation that ΔOD is proportional to $\langle N \rangle$, which indicates that the TA signal, ΔOD, is a straightforward measure of the populations of corresponding excited states.

3. Model of CT dynamics

In a PeNC-acceptor complex, the GSB dynamics after the fast hot-carrier relaxation process, is followed by an intrinsic recombination, a CT and a charge return (CR) process:

$$dN/dt = -k_{\mathrm{r}}N - k_{\mathrm{CT}}N + k_{\mathrm{CR}}N^* \qquad (2)$$

where N^* denotes the population of charged particles after the CT process, k_{r}, k_{CT} and k_{CR} are rates for charge recombination, CT and CR processes, respectively. We preliminarily assume a very slow CR process, $k_{\mathrm{CR}} \ll k_{\mathrm{CT}}$. This simplifies the total relaxation rate of charge carriers k on a relatively fast timescale:

$$\frac{dN}{dt} = -kN, \text{ in which } k = k_{\mathrm{r}} + k_{\mathrm{CT}} \qquad (3)$$

In practice, by measuring the intrinsic recombination rate, k_{r}, from the PeNC-only system, and the total relaxation rate k in the PeNC-acceptor complex, the CT rate can be derived by:

$$k_{\mathrm{CT}} = k - k_{\mathrm{r}} \qquad (4)$$

Based on this model, several research groups have measured the CT rates (or time constants) from PeNCs to various acceptors using TA spectroscopy. Meanwhile, **Equation 4** also explains the acceleration of bleach recovery observed in most TA investigations. For instance, **Figure 2** from Lian and coworkers' report[33] shows an obviously faster GSB recovery dynamics from $CsPbBr_3$ PeNCs in the presence of electron acceptors benzoquinone (BQ) and hole acceptors phenothiazine (PTZ) than free $CsPbBr_3$ PeNCs, even though the spectral signatures remain unchanged. Furthermore, the GSB feature of pure $CsPbBr_3$ PeNCs was demonstrated to show nearly mono-exponential recovery kinetics with a time constant of 4.5±0.2 ns, which is dominated by the electron-hole recombination process. In the presence of the CT process, the GSB recovery becomes shorter and complicated. Multi-exponential fittings yield the half-lives of 65±5 ps and 49±6 ps for electron transfer (ET) and hole transfer (HT) processes, respectively.[33]

In fact the kinetics of the GSB signal in usual PeNC-acceptor complexes may be influenced by many processes. Shen et al. calculated that the electron injection efficiency from $CsPbI_3$ PeNC to TiO_2 can reach ~99% under a low excitation intensity, by considering carrier recombination rate, one-body trapping rate, and the derived CT rate.[34] As the excitation intensity increases, the GSB recovery kinetic becomes more complicated under influence of

the multi-exciton effect. Samanta et al. revealed that the biexciton Auger recombination should be responsible for the acceleration of GSB dynamics for $CsPbI_{3-y}Cl_y$ (chloride-doped $CsPbI_3$) PeNCs at higher pump fluence (Figure 2c).[35] Interestingly, the biexciton can be extracted from $CsPbI_{3-y}Cl_y$ PeNCs using electron acceptor C_{60}, as revealed by comparing the GSB kinetics in the absence and presence of C_{60} at different pump laser fluences (Figure 2d).

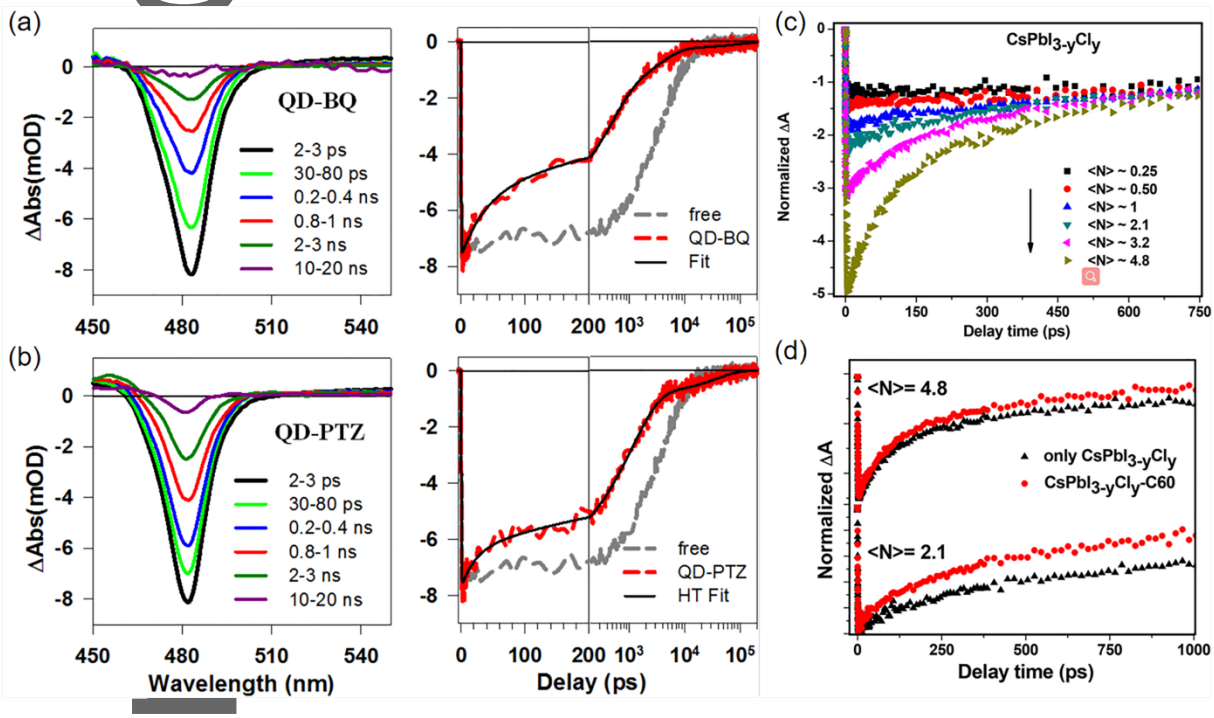

Figure 2. (a) TA spectra of $CsPbBr_3$ PeNC-BQ and $CsPbBr_3$ PeNC-PTZ complexes and (b) corresponding bleach kinetics in comparison with free $CsPbBr_3$ PeNCs after 400 nm excitation. Black solid lines are multi-exponential fits to the kinetics. Reproduced with permission.[33] Copyright 2015, American Chemical Society. (c) Bleach recovery kinetics of (c) $CsPbI_{3-y}Cl_y$ PeNCs as a function of excitation laser fluence and (d) $CsPbI_{3-y}Cl_y$ PeNCs in the absence and presence of C_{60} at different pump laser fluences. Reproduced with permission.[35] Copyright 2018, American Chemical Society.

In contrast, to probe the kinetics of the characteristic spectra of charged acceptors may be a more straightforward way of characterizing k_{CT}. However, to date few investigations have

reported the observation of either GSB or PIA signals for charged acceptors.[36-38] We summarize several factors that should be responsible for such a lack of appropriate data. Firstly, both GSB and PIA signals for acceptors may overlap with the broad band PIA signals of PeNCs, or be out of the wavelength range of the probe spectrum. Secondly, the acceptors usually possess a relatively low light absorption cross section compared to the PeNC donors. This means that the GSB and PIA signals of acceptors are inherently weak and easily overwhelmed by the spectral features of PeNCs. Finally, in order to eliminate multi-exciton excitation that may complicate carrier relaxation and transfer processes, the measurements are generally carried out under low excitation fluence conditions, which further weakens the characteristic spectra of acceptors. However, even applying intensive excitation, the CT process may be modulated by the significant Auger process that usually involves excitation of a third charge carrier leading to a complicated CT process.

The semiclassical Marcus theory provides a quantum description of the CT reaction in a weak electronic coupling regime,[39, 40] which is adaptive to common CT processes from a typical PeNC complex. k_{CT} is quantified by:

$$k_{CT} = \frac{2\pi}{\hbar}|H_{DA}|^2 \frac{1}{(4\pi\lambda k_B T)^{1/2}} \exp\left(-\frac{(\lambda+\Delta G^0)^2}{4\lambda k_B T}\right) \qquad (5)$$

This theory reveals that the CT process is driven by the change of the free energy ΔG^0 of the complex system. The electronic coupling H_{DA}, between the charge donor and acceptor is usually determined by the extension of the charge wavefunction to the acceptor. The reorganization energy λ may modulate the driving force and lead to an inverted regime in which large ΔG^0 results in slow k_{CT} that is contrast to the intuitive prediction. Over the past

decades, intensive effort has been devoted to II-VI nanomaterials upon the dependence of k_{CT} on these three parameters. Some simulation works proved the reliability and validity of the Marcus theory model. At the same time, a limitation was also pointed out that the Marcus inverted region, an essential regime for molecular and bulk semiconductor systems, is absent in these cases over an apparent driving force.[41] It is also worth noting that the Auger-assisted ET (AAET) pathway may complement the Marcus rules especially under obvious quantum confinement conditions. The AAET involves excitation of additional electrons when CT occurs. This leads to enhancement of CT rates and an absence of the inverted regime with large driving force.[39]

Besides, the Marcus theory model may contemplate the dimensionality effect in the CT process in terms of the extension of the charge wavefunction at donor-acceptor interface. The dimensionality effect on CT rates between $CsPbBr_3$ and CdSe was evaluated in Schaller and coworkers' study[42] by comparing their electronic interactions in the dimensional combinations of 0D-0D, 0D-2D and 2D-2D structures. Faster CT rate from $CsPbBr_3$ NCs to CdSe nanoplatelets (NPLs) than CdSe QDs was revealed by using TA spectroscopy, and was speculated to stem from the extended wavefunctions of the acceptor states. Furthermore, Mohammed et al. demonstrated that in $MAPbBr_3$ PeNC-acceptors (tetracyanoethylene) the dimensionality is able to tune the CT dynamics at the interface.[43] These findings offer potential implications in maximizing the CT rates in in optimal designs of photovoltaics devices. Nevertheless, evaluation of the dimensionality effect remains complicated, as the other factors such as CT driving force and interparticle distance may also be altered with changes of the particle dimensionality.

In contrast to the II-VI nanomaterials, all inorganic $CsPbX_3$ PeNCs have received less attention on the fundamental principles of the CT process to date. Some work has reported a size-dependence of the CT rate in going from $CsPbI_3$ PeNCs to TiO_2 and rationalized it by Marcus ET theory.[34] Although carrier dynamics in PeNCs may still undergo a similar physical framework as conventional II-VI nanostructures, there is still a demand in systematic studies for PeNCs considering different properties including the dielectric effect, lattice structures, intrinsic carrier dynamics, surface chemistry and so on.

4. Concerns on the TA measurements of CT rates in $CsPbX_3$ PeNCs

We firstly discuss the acceptor in the CT complex system. In 2015, Lian et al. reported for the first time a detailed TA spectroscopy study of the CT process in $CsPbBr_3$ PeNCs. They demonstrated efficient electron and hole harvesting by BQ and PTZ molecules, respectively.[33] Following this work, myriad potential acceptors have been investigated. These acceptors can be generally classified into two categories, namely organic molecules and semiconductor nanoparticles. The latter includes metal oxide (MO) and conventional metal chalcogenide nanomaterials.

The large surface area of PeNCs enables direct anchorages of organic molecules. Moreover, this linking configuration can help to extend the functionality of the nano-systems by using organic molecules with diverse functional groups.[38, 44, 45] For instance, 1-aminopyrene was reported by Samanta et al. as the hole acceptor for $CsPbBr_3$ and $CsPbI_3$ PeNCs. Meanwhile the amino and pyrene moieties can play a role in surface passivation and CT promotion,

respectively.[44] This has promoted more intensive works focusing on molecular acceptors and their interactions with semiconductor nanoparticles.

According to their solubility of the molecular acceptor in the solvent of choice, the methods for assembling organic molecules onto the surfaces of PeNCs fall broadly into two categories. In the soluble case (normally referring to toluene), it is very convenient to mix organic acceptors of an appropriate amount in a PeNC suspension, and the homogeneity can be guaranteed by vigorously stirring. This method also works for low dimensional metal chalcogenide acceptors. In the work of Ghosh et al., TA measurements were carried out directly on colloidal mixtures of PeNCs and CdSe quantum dots.[46] For acceptors of poor solubility (normally in hexane), ultrasonic treatment is feasible to add molecular powder directly in the PeNC suspension. Filtration of the mixture can then be made to purify the PeNC-molecule complexes before taking spectroscopy measurements. In particular, in the study by Sum and coworkers, bathophenanthroline, the electron receptor molecule, was deposited on a spin-coated $MAPbBr_3$ PeNCs ($MA=CH_3NH_3$) film through thermal evaporation under a pressure of 10^{-6} torr.[47]

In contrast, PeNCs are usually loaded onto films of MO semiconductor nanoparticles by spin coating,[48] or immersing MO nanoparticle films in the PeNC suspension.[34, 49] Dip coating and electrophoretic deposition are also common ways to deposit traditional semiconductor NCs on MO nanoparticles. Though no report has applied to PeNCs yet, these methods are of great potentiality for assembling PeNCs with MO nanoparticles.

In addition to independent acceptors as mentioned above, $CsPbX_3$ PeNC-based heterostructures have also been synthesized and extensively studied recently with attempts to integrate new features and obtain superior material performance in terms of stability, particle dispersion and photoluminescence.[50-56] Alternatively, the semiconductor or metal heterostructure can build a close contact with PeNCs through dotting or growing into a full shell on them and thus enable more efficient transfer processes and following interfacial charge separation. For example, the heterojunction of $CsPbX_3$ PeNC-plasmonic metal combinations enables more efficient photogenerated carrier transfer between each counterpart, and exhibit promising properties in charge separation for the applications in photocatalysis and hot carrier solar cells.[55, 56] Therefore, in this Review, we also focus on $CsPbX_3$ PeNC-based heterostructures as the third type of CT system and place particular emphasis on plasmonic-induced hot ET to $CsPbX_3$ PeNCs across the heterojunction. As summarized in **Figure 3**, depending on the energy level alignments of the transfer system, the CT process occurs in different ways and gives rise to many concerns relating to the TA measurements of CT rates, as detailed in the following.

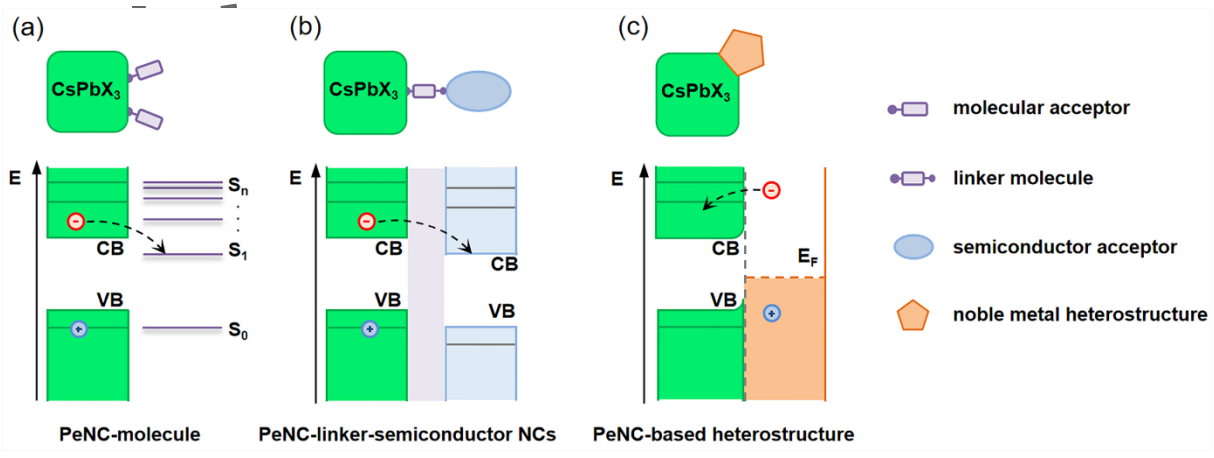

Figure 3. Schematic illustrations of various PeNC CT systems: (a) PeNC-molecule, (b) PeNC-linker-semiconductor NCs and (c) A representative case of PeNC-based heterostructures, PeNC-plasmonic metal ensembles. S_0 represents the ground state and S_n represent n^{th} excited state of the molecules; VB and CB represent the valance and conduction bands of semiconductors, respectively; E_F represents the Femi energy level of the metal.

4.1. Multiple CT pathway effect complicates measurements of the CT rates

A few reports have revealed a CT rate dependence on acceptor concentrations, in which the measured transfer rate increases with increasing concentration of acceptors.[38, 57, 58] This is ascribed to the multiple CT pathways when multiple acceptor moieties are associated with each particle (**Figure 4**a).[59] As demonstrated in Figure 4b, the GSB for $CsPbI_3$ PeNCs decays much faster initially and retains slower with an increasing number of rhodamine B (RhB) molecules adsorbed onto the PeNC surface.[60] In order to allow reliable and meaningful comparison of CT rates among different systems, the intrinsic CT rate, k_i, which is the average rate of CT for only one CT-active acceptor per particle, is applied.[60, 61] The observed decay rate for one excited particle with multiple CT pathways is assumed as:

$$k_n = k_r + nk_i \qquad (6)$$

where the subscript *n* denotes the number of CT-active acceptors binding to one particle. The binding distribution of acceptors should also be considered as a result of the uncertainty of the nanoparticle-acceptor binding process (Figure 4c). Assuming a rational Poisson distribution of binding acceptors, the probability *f*(n) of one particle with *n* absorbed acceptors is:

$$f(n) = \lambda^n \exp(-\lambda)/n! \qquad (7)$$

where λ is the average number of CT-active radicals per particle. It is noted that λ is usually smaller than the amount of added acceptor per particle, because not all added molecules will adsorb to the particle. The value of λ can be obtained from routine measurements of steady-state absorption spectra by knowing the extinction coefficients of the PeNC donor (ε_D) and molecular acceptor (ε_A):[36]

$$\lambda = \frac{I_A/\varepsilon_A}{I_D/\varepsilon_D} \qquad (8)$$

where I_D and I_A are absorbances of PeNC and acceptor derived from their steady-state absorption spectra, respectively. However, for PeNCs, it is unfeasible to determine their extinction coefficients in solution. So far the reported extinction coefficients of the $CsPbX_3$ NCs still suffer remarkably large uncertainties, thus complicating determination of λ through regular steady-state absorption spectroscopy.

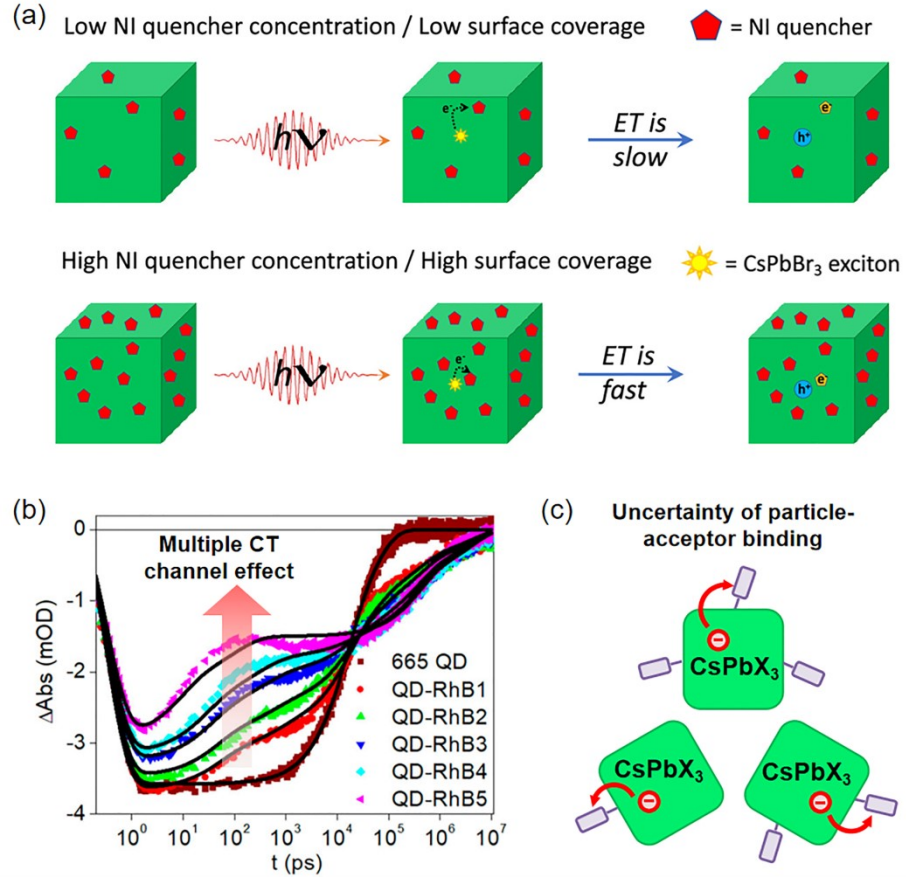

Figure 4. (a) Schematic illustration of the dependence of ET rate from $CsPbBr_3$ PeNCs on the concentration of surface-anchored naphthalimide (NI quencher). Reproduced with permission.[59] Copyright 2021, American Chemical Society. (b) An example of the effect of multiple acceptor CT channels in a $CsPbI_3$ PeNCs-RhBn complex. It shows the TA GSB kinetics of $CsPbI_3$ PeNCs, with increasing RhB loading amount (RhB1-5). Reproduced with permission.[60] Copyright 2019, American Institute of Physics. (c) Schematic of uncertainty of $CsPbX_3$ nanoparticle-acceptor binding.

Mandal et al. proposed a steady-state PL intensity dependence on varying concentrations of acceptors.[62] By assuming the inevitable PL quenching effect by the CT process, the probability of finding PeNCs without any adsorbed acceptor equals the fraction of the integrated PL intensities in the presence and absence of acceptors (PL/PL_0). This correlates

with the adsorbed acceptor to the mean fractional surface coverage on NC surface, θ, by the following equation:

$$f(0) = \mathrm{PL}/\mathrm{PL}_0 = (1-\theta)^N \qquad (9)$$

where N is the total number of binding sites per NC. Another practical way of determining λ was proposed by Weiss et al. using in-situ TA and has been applied to II-VI QDs.[61] It is assumed that: (a) any particle with one or more active acceptor radicals attached will undergo a CT process, and the GSB will recover due to the CT process; and (b) the kinetics at long delay times are separated from the CT process since the latter occurs on a short time scale. Therefore, $f(0)$, the fraction of the NCs with no acceptors in the complexes, can be determined from the ratio between the TA bleach signal for NCs without acceptors, B_0, and that in the NC-acceptor complex, B. Consequently λ is given by:

$$\lambda = -\ln f(0) = -\ln(B/B_0) \qquad (10)$$

Finally, by applying an infinite sum of exponentials, $N(\mathrm{t}) = N(0)\sum_{\mathrm{n}=0}^{\infty} f(n)\exp(-k_{\mathrm{n}}\, t)$, to fit the measured TA bleach decays combining the Poisson distribution, the intrinsic CT rate, k_{i}, can be determined:

$$N(t) = N_0 \exp\left[-k_{\mathrm{r}} t - \lambda(1-\exp^{-k_{\mathrm{i}} t})\right] \qquad (11)$$

Tkachenko et al. applied the above model to determine λ and k_{i} from PeNC systems. They also implemented a global fitting analysis of the TA spectra for $CsPbBr_3$ PeNC-AQ and $CsPbBr_3$ PeNC-C_{60} hybrids. As shown in **Figure 5**, a decay component associated with the band formation of charged acceptors (denoted as the Pois) was identified to follow this

model. They finally determined the ET time constants, $1/k_i$, for an ideal one-to-one $CsPbBr_3$ PeNC-AQ and -C_{60} complex, to be 30 and 190 ps, respectively.[38]

There is another meaningful way for comparison of CT rates by keeping similar concentrations of PeNCs and acceptors rather than knowing the exact molecule numbers. Lian et al. carefully controlled the relative concentrations of PeNC dispersion solutions, by realizing that the extinction coefficients of $CsPbBr_3$ PeNCs at short wavelengths far from their band edge were simply proportional to their volumes.[33, 63] This helps to circumvent the variance brought in by different λ values, nonetheless, the absolute ratios should be reliably known when comparing the k_{CT} from same PeNC donor to various acceptors that may possess different adsorption or binding probabilities.

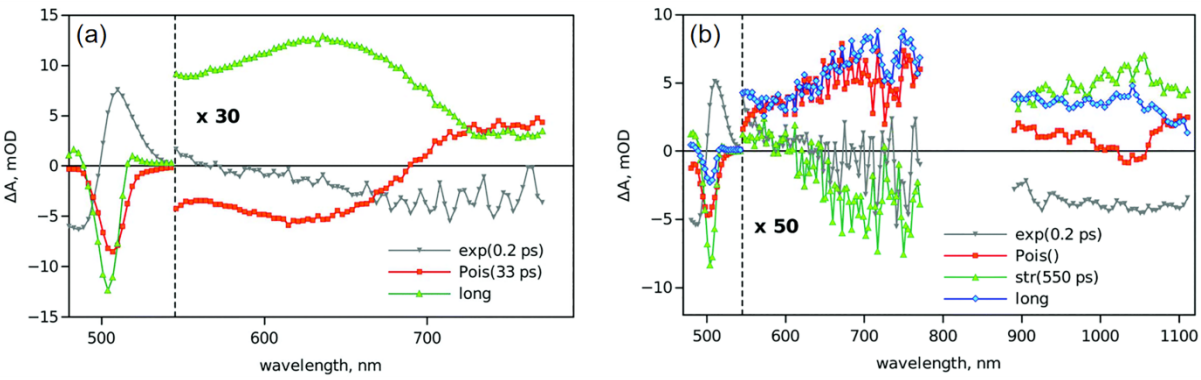

Figure 5. Transient absorption decay component spectra of (a) PeNC-AQ and (b) PeNC-C_{60} hybrids after global fitting. Excitation wavelength is 470 nm. For better visualization, the spectra at >545 nm are multiplied by 30 for PeNC-AQ and 50 for PeNC-C_{60} complexes, respectively. Reproduced with permission.[38] Copyright 2019, Royal Society of Chemistry.

The multiple CT pathway effect may also be saturated with sufficient adsorbed acceptors. In subsequent work Tkachenko et al. conducted further TA studies on multi-electron transfer reactions of $CsPbBr_3$ PeNC-AQ hybrids.[64] The transient absorption feature of the AQ anion caused by CT (600 nm) became saturated when the excitation power was elevated. It was concluded that as many as, on average, 5 electrons can be transferred from one $CsPbBr_3$ particle to surface adsorbed AQ acceptors. This scenario can be attributed to the fact that each CT process undergoes an increasing Coulomb potential barrier compared to the following one, which correspondingly decreases the CT rate and eventually ceases the following CT events (**Figure 6**a). Similarly, Wu et al. examined the multi-hole transfer dynamics by pump fluence-dependent TA measurements (Figure 6b-d). Based on the feature that the Auger signal is strongly suppressed by HT kinetics in the presence of tetracene, they deduced that, for $CsPbCl_xBr_{3-x}$ PeNCs with a Cl to Br ratio of 1 : 7, only up to 5.6 holes can be transferred from a multiply excited PeNC particle, even though 137 tetracene carboxylic acid (TCA) hole receptors are bound to its surface.[65] In fact, in a previous work, by way of pump-push-probe (PPP) spectroscopy, Wu et al. have already demonstrated a lower CT efficiency from positively charged $CsPbBr_3$ PeNCs to RhB as compared to neutral NCs.[36] Moreover, the new CT process also has to compete with Auger recombination of charged multiexcitons. As a result, the CT saturation effect should be carefully considered in situations where abundant acceptors are added to the nanoparticle solution.

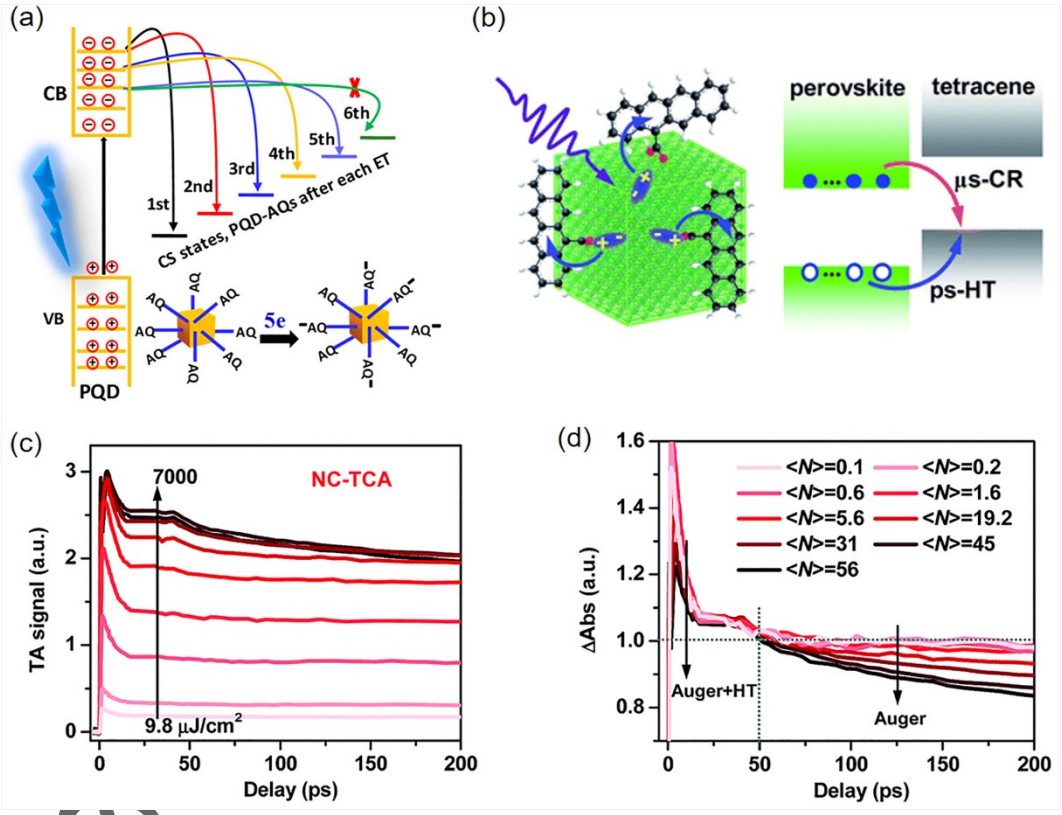

Figure 6. (a) Schematic illustration of the saturation of multiple ET processes. Reproduced with permission.[64] Copyright 2019, American Chemical Society. (b) Schematic representation of the band alignment for hole transfer and charge recombination from $CsPbCl_xBr_{3-x}$ PeNCs with a Cl to Br ratio of 1 : 7 to tetracene carboxylic acid (TCA). (c) Pump-fluence dependent GSB kinetics of PeNC-TCA complexes. (d) Normalized plots in (c) in the delay range of 20-50 ps. <*N*>: the average exciton numbers at these fluences. Reproduced with permission.[65] Copyright 2019, Royal Society of Chemistry.

4.2. Surface ligand effects on CT process

Surface ligands also play a role in determination of the CT process, especially in the non-direct contacting complexes such as PeNC-linker-TiO_2, where the ligands act as the linker to introduce mutual interactions between the donor and acceptor. The common long-chain ligands such as oleylamine (OAm) and oleic acid (OA) are typical insulators and may act as a tunneling barrier that slows down the transfer rate. By TA spectroscopy, Lian et

al. compared two batches of $CsPbI_3$ PeNCs with different extents of a post-synthesis washing treatment. They found that $CsPbI_3$ PeNCs with a lower OAm and OA coverage density (washed twice) show more pronounced charge separation performance at the PeNCs/TiO_2-particle interface compared with the pristine samples (**Figure 7**a).[66] In order to achieve both effective surface passivation and efficient charge extraction, careful control of ligand density has been intensively emphasized in the preparation of PeNC-based photovoltaic and photoelectronic devices.[67-69]

Moreover, the electronic coupling in the hybrid system is susceptible to the length,[70, 71] anchoring group,[44] conductivity[45, 72, 73] and dipole moments of the ligands.[74] To date intensive studies have been carried out both upon hybrid MA-, FA-($FA=CH(NH_2)_2$)based and all inorganic $CsPbX_3$ PeNCs. With a focus on the chain length of the alkylamine ligand, Masuhara et al. identified an optimized chain length of five carbon atoms for balancing electronic transportation properties and durability of $MAPbBr_3$ PeNC thin films.[70] In comparison, Zhang et al. regulated the chain length of both alkylacid and alkylamine ligands on the surface of $MAPbBr_3$ PeNCs and showed the combination of octylamine and caprylic acid was favorable to both charge transport efficiency and lattice stability.[71]

In terms of the conductivity of ligands, given the insulating properties of aliphatic ligands, conductive molecules have attracted great interest for their prospective potential in enhancing inter-particle electronic coupling and thereby boosting CT rates. A 22-fold enhancement in charge mobility in comparison to conventional OA-capped $MAPbBr_3$ was firstly realized by using a common conjugated alkylamine PPA (3-phenyl-2-propen-1-amine) to cap $MAPbBr_3$

PeNCs.[45] Zhang et al. have provided systematic insights into the effects of aromatic ligands on CT processes in $MAPbBr_3$ PeNCs.[72] Not surprisingly, this strategy also works well for all inorganic $CsPbX_3$ PeNCs. Conjugated molecules including phenethylamine and PPA were introduced into $CsPbBr_3$ and $CsPbI_3$ PeNCs, and succeeded in promoting carrier transportation as well as improving the performance of $CsPbX_3$ (X=Br or I)-based light-emitting diodes.[73] In our recent work, we realized modulation of the ET rates from $CsPbBr_3$ PeNCs to TiO_2 by use of different types of anchored surface ligands. Application of aromatic ligands such as naphthalene acid showed an enhanced CT efficiency than the insulating cross-linked silicone ligands. Additional calculations of the ligand molecule frontier orbitals verified the potential-barrier effect. We suggest that an appropriate potential barrier will lead to a more efficient ET rate.[75] Li et al. reported an obvious increase in CT rates from $CsPbBr_3$ PeNCs to black phosphorus nanosheets in the presence of the aromatic ligands benzylamine and benzoic acid.[76] However, it should be noted that the use of conjugated ligands introduces a dilemma for the synthesis of uniform and high quality PeNCs. In addition, far less is known about the conjugated ligand chemistry on crystal growth and stabilization of the $CsPbX_3$ PeNCs in comparison with commonly applied ligands. The dependence of stability and electronic transportation properties of $CsPbX_3$ PeNCs on capping ligands still need to be investigated in detail.

Being similar to the ligand effect, the inorganic capping shells in heterostructures of $CsPbBr_3$ PeNCs also show a modulation effect on CT processes. For example, electronic coupling can be tuned by using inorganic shells of different thicknesses. Buonsanti et al. applied an AlO_x shell as the spacer between $CsPbBr_3$ PeNCs and CdSe NPLs (Figure 7b).[77] With increasing

AlO_x shell thickness, the predominant electronic transfer mechanism in this system was shown to be gradually replaced by Förster resonance energy transfer, which indicates a negligible CT process at the larger donor-acceptor separation (Figure 7c). Some cadmium-based shells, such as CdS may not only offer $CsPbBr_3$ PeNCs improved the stability in polar solvents but also allows for a type II band alignment and facilitates long-lived charge separation.[78] Nevertheless, the electronic transmission efficiency is still limited by the uncontrollable loading position and lattice mismatch-directed defects.

Recently, the 2D perovskite nanostructures has also been extensively explored. The 2D perovskite nanostructure, or NPLs, in which the inorganic metal-halide perovskite layers are sandwiched between organic ligand layers, may form multiple quantum well (QW) potentials. Therefore, the organic ligands play an important role in the CT process in 2D NPLs. The perovskite QWs can be accordingly tuned by using different ligands. One of the attractive properties is the available typical type II band alignment in perovskite NPLs which may lead to efficient charge separation.[79-83] It is found that the charge separation properties of perovskite NPLs are closely correlated with the NPL thickness,[81] the acceptor contractions[82] and organic cation size.[83] Meanwhile, the energy barrier formed by the insulating ligands between QWs will induce poor interlayer carrier transport. Jin et al.[79] reported an Auger-assisted QW-to-QW ET process in $(C_mH_{2m+1}NH_3)_2PbI_4$ perovskite NPLs particularly with m = 12 and 18, where the energy barrier is close to the QW band gap. This provides a new strategy for designs of 2D perovskite structures with improved interlayer charge mobility, which is essential to advance their applications in optoelectronic devices.

Besides spacing or the conducting effect, surface chemistry or physics by ligands may also affect the CT process in $CsPbX_3$ PeNCs. Kamat et al. carried out TA spectroscopy measurements to explore interfacial ET reactions from $CsPbBr_3$ PeNCs to methyl viologen for photocatalytic applications.[84] They observed a much longer sustained bleaching signal of the PeNCs in the presence of methyl viologen, which is induced by a dipole created by holes and electrons residing in $CsPbBr_3$ PeNCs and methyl viologen (Figure 7d). In their following work, they further examined the ET process under the influence of three different $CsPbBr_3$ PeNC surface chemistries, including prototypical OA/OAm ligands, $PbSO_4$-oleate capping, and didodecyldimethyl-ammonium bromide (DDAB) ligands (Figure 7e).[85] As measured from TA spectroscopy (Figure 7f-h), the CT rate and overall efficiency from $CsPbBr_3$ PeNCs to methyl viologen were sensitive to ligand-assisted surface interactions because each surface ligand varies in the capability of stabilizing the ET product. Interestingly, Oron et al. observed a nano-p-n junction analog in similar $CsPbBr_3$ PeNCs/CdSe NPLs hybrids, in which the interfacial dipole of molecular linkers (p-Aminobenzoic acid and Glycine) induces an equilibrium charge transfer process between $CsPbBr_3$ and CdSe without photoexcitation.[74]

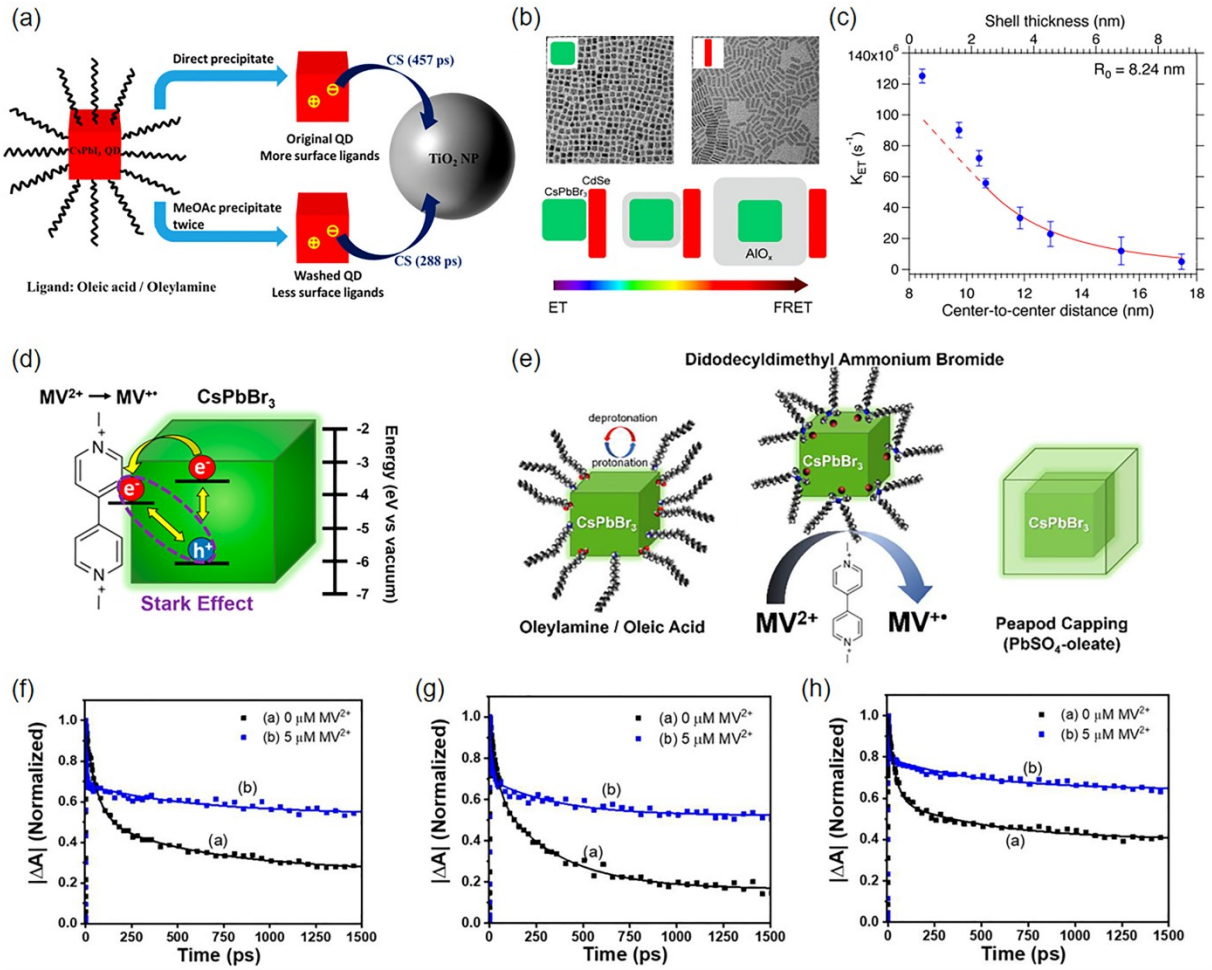

Figure 7. (a) Illustration of post-synthetic treatment effect on the charge separation (CS) processes at the interface of $CsPbI_3$ PeNCs and TiO_2 nanoparticles. Reproduced with permission.[66] Copyright 2019, American Chemical Society. (b) Shell thickness-modulated electronic interactions between the $CsPbBr_3$ NCs and the CdSe nanoplatelets from electron to energy transfer. (c) Energy-transfer rates versus the center-to-center distance calculated for the different AlO_x shell thicknesses. Reproduced with permission.[77] Copyright 2020, American Chemical Society. (d) Schematic illustration of a long-lived charge-separated state following band gap excitation, which arises from the creation of a dipole with the hole residing in $CsPbBr_3$ and the electron in the surface-bound methyl viologen moiety. Reproduced with permission.[84] Copyright 2019, American Chemical Society. (e) $CsPbBr_3$ PeNCs with oleic acid/oleylamine (OA/OAm), $PbSO_4$-oleate, and didodecyldimethylammonium bromide (DDAB) surface chemistries. (f-h) TA decay kinetics for $CsPbBr_3$ NCs without MV^{2+} and with 5 μM MV^{2+} for the three nanocrystal surface chemistries. Reproduced with permission.[85] Copyright 2020, American Chemical Society.

It can also be seen that the surface capping ligands may place synthetic influence on the CT process. More comprehensive analysis is required to elucidate the ligand effect and the corresponding mechanism. From the more practical perspective of macroscopic optoelectronic properties of PeNC-based devices, by using different ligand linkers, it is feasible to enable better control of both the chemical stability and electronic transportation properties of PeNCs.

Table 1 summarizes the CT rates or time constants of $CsPbX_3$ PeNCs reported to date. We specifically focus on the results from TA measurements. The pump wavelength, if not otherwise specified, is 400 nm. To allow ease of reference, Table 1 also provides the donor-acceptor ratio (or the average number of CT-active radicals per donor particle, n) and the edge length or diameter of PeNC donor, if available. We also accordingly plot the reported CT time constants $CsPbX_3$ PeNCs and seek possible law that reveals different CT processes with different type of acceptors, as shown in **Figure 8**. It indicates a rough rule that molecular acceptors may induce a faster CT process meanwhile semiconductor type acceptors generally involve longer transfer processes with a time constant range over tens of nanoseconds. We suggest the trend may be rationalized by the ligand-bridge effect that acts as an energy barrier slowing down the CT rates in PeNC-linker-semiconductor complexes. Hot carrier transfer obviously occurs on a much faster timescale that should be comparable to the fast hot carrier relaxation process. PeNC heterostructures are more affected by the energy assignments of the hetero-materials that may possibly induce plasmonic (metal) or carrier delocalization (semiconductor such as CdSe) effect.

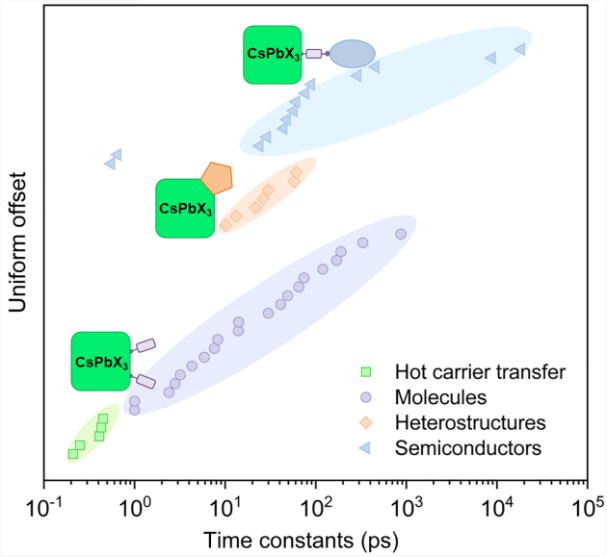

Figure 8. Summary of reported CT time constants in Table 1. The time constants for each type acceptor are evenly offset in y-direction in an ascending order, in order to clearly distinguish the different types of CT systems. Color shades indicate the same category of CT systems as presented in Table 1.

Table 1. Summary of CT rates or time constants of $CsPbX_3$ PeNCs. (ET: electron transfer; HT: hole transfer; HET: hot electron transfer; HHT: hot hole transfer; L: long edge, S: short edge)

	Ref.	Donor PeNCs-Acceptor	Edge length/ Diameter [nm]	Time constants /CT rates (pump wavelength)
molecule	[44]	$CsPbBr_3$/$CsPbI_3$-1-ampinopyrene	8.0±0.5/10±0.5	HT: 120 ps (470 nm) /170 ps (530 nm)
	[36]	$CsPbBr_3$-Rhodamine B (n=52)	10.1±1.0	ET: 74.3±3.2 ps & 472.6±5.3 ps
			11.8±1.6	ET: 872±52 ps (500 nm)
	[60]	$CsPbI_3$-Rhodamine B	10.8±1.5	ET: 331±23 ps (500 nm)
			6.5±1.1	ET: 40.6±4.3 ps (500 nm)
	[65]	$CsPbCl_xBr_{3-x}$ (Cl:Br=1:7)-tetracene (n=137)	8.0~10.0	ET: 7.6±0.2 ps (340 nm)
	[33]	$CsPbBr_3$-BQ/PTZ	7.4±1.3 (L) 6.0±1.0 (S)	ET: 65±5 ps/HT:49±6 ps,
	[37]	$CsPbBr_3$-(4,5-dibromofluorescein)	7.35±1.3 (L) 6.80±1.2 (S)	HT:1~1.25 ps
	[38]	$CsPbBr_3$-anthraquinone/C_{60} (1:1)	9.0±0.5	ET : 30±3 ps/190±60 ps (470 nm)
	[64]	$CsPbBr_3$-anthraquinone (1:20)	9.0±0.5	ET: 1 ps (470 nm)
	[85]	$CsPbBr_3$-MV^{2+}(ligand: OA/OAm)	—	ET:3.6×10^{11} s^{-1} (387 nm)
		$CsPbBr_3$-MV^{2+}(ligand: $PbSO_4$-oleate)		ET:1.2×10^{11} s^{-1} (387 nm)
		$CsPbBr_3$-MV^{2+}(ligand: DDAB)		ET:2.3×10^{11} s^{-1} (387 nm)
	[86]	$CsPbBr_3$-(phenyl-C_{61}-butyric acid methyl ester) ($CsPbBr_3$ film thickness: 65/45/35/25 nm)	12±1	ET: 14.1/ 5.9/ 3.2/2.4 ps
	[87]	$CsPbBr_3$-TpyP	12± 0.4	HHT: 4.76×10^{12} s^{-1} (370 nm) HHT: 3.96×10^{12} s^{-1} (400 nm) HHT: 2.22×10^{12} s^{-1} (450 nm)
	[88]	$CsPbBr_3$-MTH	—	HHT: 2.3×10^{12} s^{-1} (350 nm) HT : 7.1×10^{10} s^{-1} (350 nm)
duct	[48]	$CsPbBr_xCl_{3-x}$-TiO_2	—	ET: 89 ps

[49]	$CsPbBr_3$-TiO_2	—	ET:2.28×10^{10} s^{-1} (387 nm)
	$CsPbBr_3$-ZnO		ET:3.44×10^{10} s^{-1} (387 nm)
	$CsPbBr_3$-SnO_2		ET:4.25×10^{10} s^{-1} (387 nm)
	$CsPbBr_3$-ZrO_2		—
[89]	$CsPbBr_3$-TiO_2	18	ET:5.4×10^{7} s^{-1}
	$CsPbBr_3$-SnO_2		ET:1.14×10^{8} s^{-1}
	$CsPbBr_3$-SiO_2		—
[34]	$CsPbI_3$-TiO_2	10	ET: 2.10×10^{10} s^{-1} (470 nm)
		12	ET: 1.76×10^{10} s^{-1} (470 nm)
		15	ET: 1.30×10^{10} s^{-1} (470 nm)
[66]	orignal $CsPbI_3$/washed $CsPbI_3$-TiO_2	13.5±2.7/14.3±3.3	ET: 457±4 ps/288±1 ps (500 nm)
[46]	$CsPbBr_3$-CdSe/CdSe@CdS	10	ET: 550 fs ET: 650 fs
[90]	$CsPbBr_3$-ferrocenium	—	ET: 1.64×10^{10} s^{-1} (387 nm)
heterostructure			
[55]	$CsPbBr_3$-Au	8.1±1.1 (orignal)/ 8.1±1.4 (with Au)	HET: $(2.43\pm0.39)\times10^{12}$ s^{-1} ET: $(1.73\pm0.27)\times10^{10}$ s^{-1}
[91]	$CsPbBr_3$-Au	50~100	ET: 30 ps
[78]	($CsPbBr_3$-CdS)-ethyl viologen (EV^{2+},4/8/16/32 μM)	9.4±1.6	ET: $(3.8/4.6/7.6/9.8)\times10^{10}$ s^{-1}

4.3. Hot carrier transfer

In single-junction photovoltaic devices, the mutual restriction between photon flux into and voltage output sets an efficiency limit of 33% for solar energy conversion, known as the Shockley-Queisser limit.[92] In a thermodynamic perspective, excess energy harvesting from hot carriers makes it feasible to transcend the Shockley-Queisser limit and achieve a maximum efficiency up to 66%.[93, 94] Exploitation of both the transport[95-97] and extraction of hot carriers[47, 62, 98] is possible in practical applications, endowing potential for developing hot carrier solar cells. The observation of unusually slow hot-carrier cooling processes in

perovskite materials, especially in $CsPbX_3$ PeNCs,[47, 99-101] has stimulated the following studies of hot carrier transfer. Slowing down the cooling rate combined with efficient extraction of hot-carrier still remains challenging in order to realize notable excess energy harvest.

Recent research has also been investigating hot carrier relaxation dynamics in bulk or low-dimensional perovskites by using TA spectroscopy.[101-107] The "hot-phonon bottleneck",[108, 109] Auger heating,[107] large polaron screening effect,[110] and acoustical-optical phonon upconversion[111] etc. have been proposed to be responsible for the unusually slow hot-carrier cooling process in perovskite materials. Specifically, the hot-phonon bottleneck and Auger heating are more likely to occur under the quantum confinement effect. Sum et al. demonstrated that the energy loss rate of $MAPbBr_3$ PeNCs decreases with reducing particle size.[47] Also, composition-dependent relaxation rates of hot carriers were observed in PeNC systems.[105, 112] In particular, it has been revealed that the cooling process occurs on a slower timescale for $CsPbX_3$ PeNCs than their organic counterparts, as a consequence of less carrier-LO phonon coupling via Fröhlich interactions with the isotropic Cs cation in the perovskite lattice.[112]

It is worthy of attention that, in TA measurements, high pump fluence may significantly enhance hot-phonon bottleneck and Auger effects. However, under sunlight illumination conditions, initial carrier density (equivalent carrier density $\approx 10^{17}$ cm^{-3}) may not be high enough to induce such effects that are favorable in slowing down the hot carrier cooling rate. Although solar concentrators have been proposed in order to realize high carrier density in

the designed device structure of hot-carrier solar cells, there is still demand for strategies to prolong the hot carrier relaxation lifetime of PeNCs at low photoexcitation levels.

A few works attempted to realize retardation of the hot carrier cooling process in perovskites with relatively low carrier densities. Since the incorporation of different ions in perovskites would modify both the electronic states and carrier effective masses, ion doping is able to modulate the intrinsic hot carrier relaxation lifetime of PeNCs.[113-115] For instance, the work from Xing et al. showed that Zn^{2+} doping in $CsPbI_2Br$ film can induce a slower hot carrier relaxation lifetime, as revealed by TA spectroscopy and theoretical calculations.[114] Zheng and coworkers demonstrated the effect of doped Mn^{2+} ions on hot carrier cooling relaxation dynamic in $CsPbI_3$ nanocrystals and their dependence on photoexcitation energy and doping concentrations.[115] Recently, Patra et al. has found a 2-time longer hot-carrier lifetime in $CsPbBr_3$-PbSe heterostructure NCs than $CsPbBr_3$ PeNCs at low excitation intensity (≈ 10^{17} cm^{-3}).[116] The less efficient conversion of LO (longitudinal optical) phonon modes into LA (longitudinal acoustic) caused by the formation of the heterostructure is responsible for the retarded hot carrier relaxation. The large specific surface area of PeNCs increases the role organic ligands can play on hot carrier cooling. Recently, by means of TA spectroscopy, we have reported a 3-fold reduced hot carrier cooling rate in $CsPbBr_3$ PeNCs capped with a cross-linked polysiloxane in comparison to conventional alkyl-chain OAm ligands, and rationalized this phenomenon based on a damped oscillation model.[117]

To date studies on the harvest of hot-carriers in $CsPbX_3$ PeNC systems are still insufficient. To achieve effective hot carrier transfer, strong wavefunction coupling between the PeNC

donor and hot carrier acceptors, suitable band alignment, and rapid hot carrier transfer rate to compete with intrinsic ultrafast excess energy relaxation are necessary. A few reports observed hot carrier transfer in $CsPbX_3$ PeNCs with some particular molecular[87, 88] or metal chalcogenide[118] acceptors. By using complementary TA and fluorescence up-conversion measurements, Samanta et al. measured a hot HT efficiency of ~43% from $CsPbBr_3$ PeNCs to 4-mercaptophenol (MTH).[88] In their study, a postprocess procedure was introduced to replace OA and OAm ligands with MTH in $CsPbBr_3$ PeNCs. Meanwhile the band alignment of MTH allows hole hopping at interfaces as shown in **Figure 9**a. From the band-gap bleach formation of PeNCs on the sub-ps timescale after above-band-edge excitation (Figure 9b), $CsPbBr_3$-MTH hybrids show a faster rising signal than $CsPbBr_3$ PeNCs, indicating the occurrence of hot HT that led to the observed faster hot hole relaxation process to the band-edge level of PeNCs. Thus, the lower peak bleach amplitude at early times (Figure 9c) indicates the hot HT efficiency of ~43%. Following the same theme, Patra and coworkers later demonstrated a hot hole extraction efficiency of ~42% from $CsPbBr_3$ PeNCs to 5,10,15,20-tetra(4pyridyl) porphyrin (TpyP) molecules.[87] In addition, they calculated the hot carrier temperature (T_c) by applying a simple Maxwell-Boltzmann distribution approximation of non-equilibrium carriers to fit the high-energy tail of the bleach signal. As shown in Figure 9d and e, the presence of TpyP molecules induced a significantly lower initial T_c followed by a faster cooling rate in comparison to the pristine $CsPbBr_3$ PeNCs, confirming the occurrence of efficient hot HT. In another study by Ghosh et al., a more rapid hot ET, even faster than the pulse-duration of 100 fs, was reported in $CsPbBr_3$ NCs-CdSe@CdS NCs composites through similar TA analysis.[46]

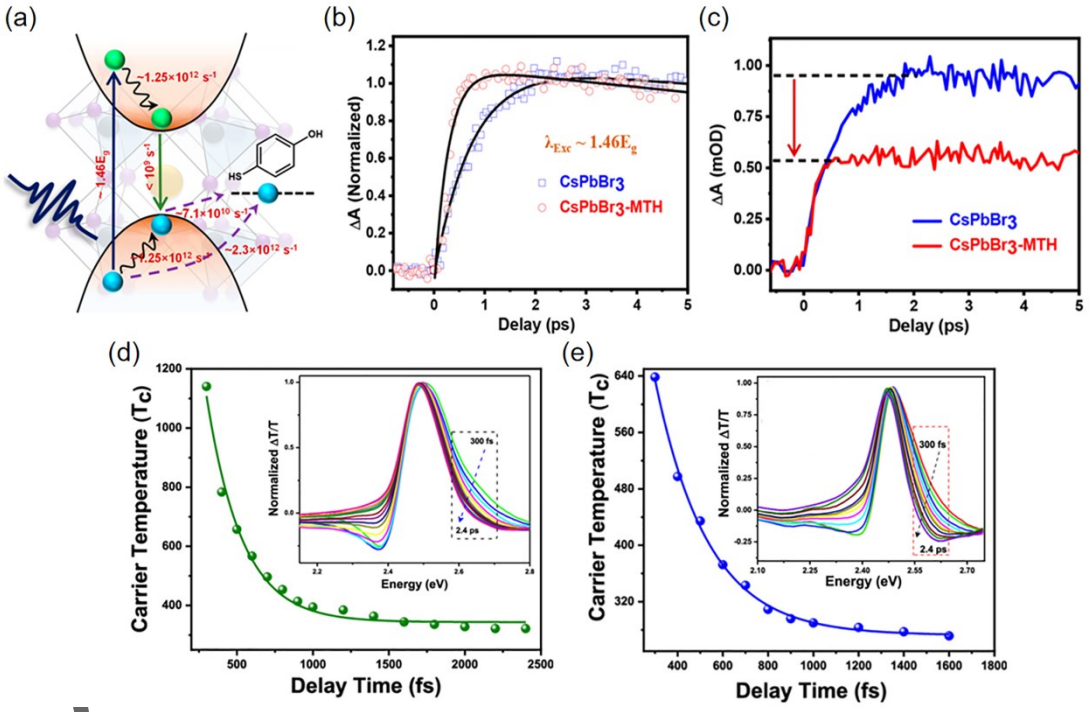

Figure 9. (a) Schematic illustration of carrier relaxation dynamics in photoexcited (350 nm, ~1.46 E_g. E_g is the band gap of the PeNCs) $CsPbBr_3$-MTH PeNCs. (b,c) Bleach formation kinetics of $CsPbBr_3$ and $CsPbBr_3$-MTH PeNCs upon excitation at 350 nm. Reproduced with permission.[88] Copyright 2020, American Chemical Society. Time-dependent carrier temperature profiles for (d) $CsPbBr_3$ NCs and (e) $CsPbBr_3$-TpyP NCs. Inset: normalized TA spectra with varying delay times (from 300 fs to 2.4 ps). Adapted with permission.[87] Copyright 2021, American Chemical Society.

However, there still exists a lack of consensus on the analysis of hot carrier parameters from TA data, in particular the use of the common approach of fitting the high-energy tail of the TA bleach signal. Sum et al. developed a more rigorous and consistent approach by globally fitting the TA spectra accounting for bandgap renormalization and spectral linewidth broadening effects (**Figure 10**a).[102] This method extracts T_c as well as other important parameters such as the quasi-Fermi levels simultaneously (Figure 10b).

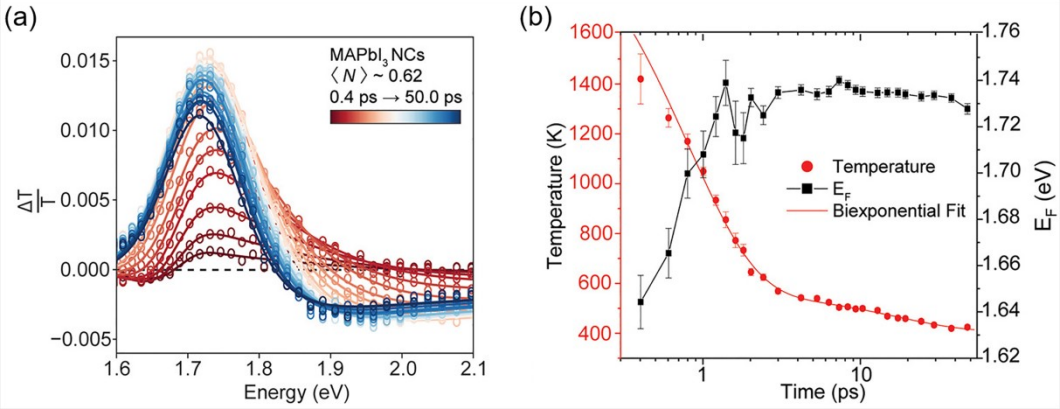

Figure 10. (a) Fits of the TA spectra of $MAPbI_3$ PeNCs at different delays with a band-filling model to determine T_c. (b) Time dependence of the quasi-Fermi energy, E_F, and T_c extracted from the fitting for $MAPbI_3$ PeNCs. Reproduced with permission.[102] Copyright 2020, American Chemical Society.

Instead of using a visible probe, Mandal et al. applied time-resolved terahertz spectroscopy (TRTS) to reveal the hot charge carrier transfer dynamics, since convention visible TA is unable to provide straightforward information on the hot state population because the hot carriers usually contribute to the non-visible band filling signals.[62] The terahertz technique measures the photoconductivity that is proportional to the overall carrier density. However, TRTS is limited by its sub-picosecond temporal resolution. These authors observed an efficient hot ET/HT within a timescale shorter than 300 fs.[62]

Recently, push-pump-probe (PPP) TA spectroscopy, developed from basic TA spectroscopy, was adopted to probe HC extraction. As illustrated in **Figure 11**a and b, in comparison to conventional pump-probe TA spectroscopy, an additional push pulse after the first excitation pulse re-excites the excited state population to higher excited states.[98] It thus allows such ultrafast transient states to be directly probed, which helps to circumvent complexities induced by multiband excitation and multiparticle effects. With PPP TA, Sum et al. realized

and observed hot carrier extraction between $MAPbI_3$ and Bphen, in which an interfacial barrier existed and allowed the re-excited electrons to be extracted by the push pulse (Figure 11c).[98] As a result, the sharp push-induced fast decay completely vanished (Figure 11d). Evidently, PPP spectroscopy is a more straightforward way of revealing hot carrier extraction mechanisms and therefore its future application in $CsPbX_3$ PeNC-based hot carrier extraction systems is expected to gain prevalence.

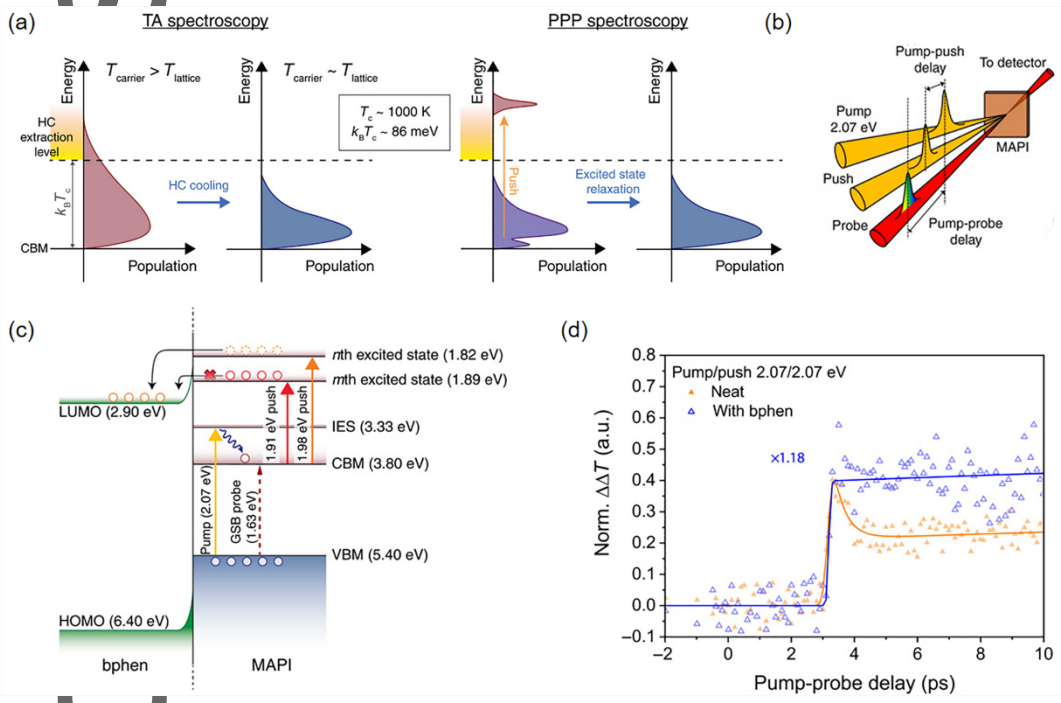

Figure 11. Schematic illustrations of (a) carrier population under probe in TA and PPP spectroscopy and (b) experimental alignment of PPP spectroscopy. (c) The influence of varying push photon energies on the thermalized carriers. Injection of HCs to Bphen occurs if the push photon energy overcomes the band offset and the interfacial barrier of Bphen. IES: initial excited state; HOMO, highest occupied molecular orbital; LUMO, lowest unoccupied molecular orbital. (d) PPP ΔΔT push-induced transients probed at GSB (760 nm) for $MAPbI_3$ without (orange solid symbols) and with Bphen (blue open symbols) acceptor layer. The 2.07 eV push pulse (15 μJ cm^{-2}) arrives 3 ps later after the 2.07 eV pump (5 μJ cm^{-2}). Reproduced with permission.[98] Copyright 2019, American Association for the Advancement of Science.

In addition, the localized surface plasmon resonance (LSPR) effect in noble metallic nanostructures arising from collective oscillations of their conduction electrons can directly convert photons into electrical energy by generating hot electrons.[119, 120] In this aspect of hot carriers, $CsPbX_3$ PeNC-noble metal heterostructures have attracted increasing attention for possible exciton-plasmon coupling. Both $CsPbBr_3$-Au and $CsPbBr_3$-Ag nanocomposites have been successfully fabricated, and some work studied the LSPR induced hot electron dynamics by TA measurements.[55, 56, 91] A schematic for the synthesis of $CsPbBr_3$-Ag hybrid NCs is shown in **Figure 12**a. Small Ag nano-particles are generated on the surface of $CsPbBr_3$ PeNCs by decomposition of AgBr under ultraviolet illumination. Xiao et al. selected a pump wavelength (420 nm) to resonantly excite $CsPbBr_3$-Ag nano-heterostructures to the LSPR. An additional bleaching signal, a consequence of LSPR, emerges at 424 nm (Figure 12b).[56] Triggered by the excitation of the LSPR, the bleaching band (XB) signal of $CsPbBr_3$-Ag hybrid NCs exhibited an upward tendency in amplitude persisting over the first 20 ps after excitation, which is much longer than observed under off-resonant excitation (Figure 12c). This can be naturally assigned to efficient plasmon-hot electron conversion at the heterojunction interface. The possible conversion pathways including plasmon-induced hot ET (PHET), charge-transfer transition (PICTT) and resonant energy transfer (PIRET) processes are schematically depicted in Figure 12d. The PHET pathway was confirmed from an additional ultrafast decay component that appeared in the signal from hybrid Ag-$CsPbBr_3$ NCs in comparison to neat Ag nanoparticles when probed near the LSPR wavelength of Ag (Figure 12e).

Highly efficient plasmon-hot electron conversion and the resultant lifetime extension of hot carriers suggest that $CsPbX_3$ PeNC-noble metal heterostructural materials exhibit promising potential to bring significant improvement in achieving hot carrier solar cells. However, the plasmonic and excitonic interactions can be quite involved. Besides, hot carrier transfer behavior is pump wavelength dependent and multiple channels including PHET, PICTT and PIRET may account for the population of hot electrons in $CsPbX_3$ PeNCs.

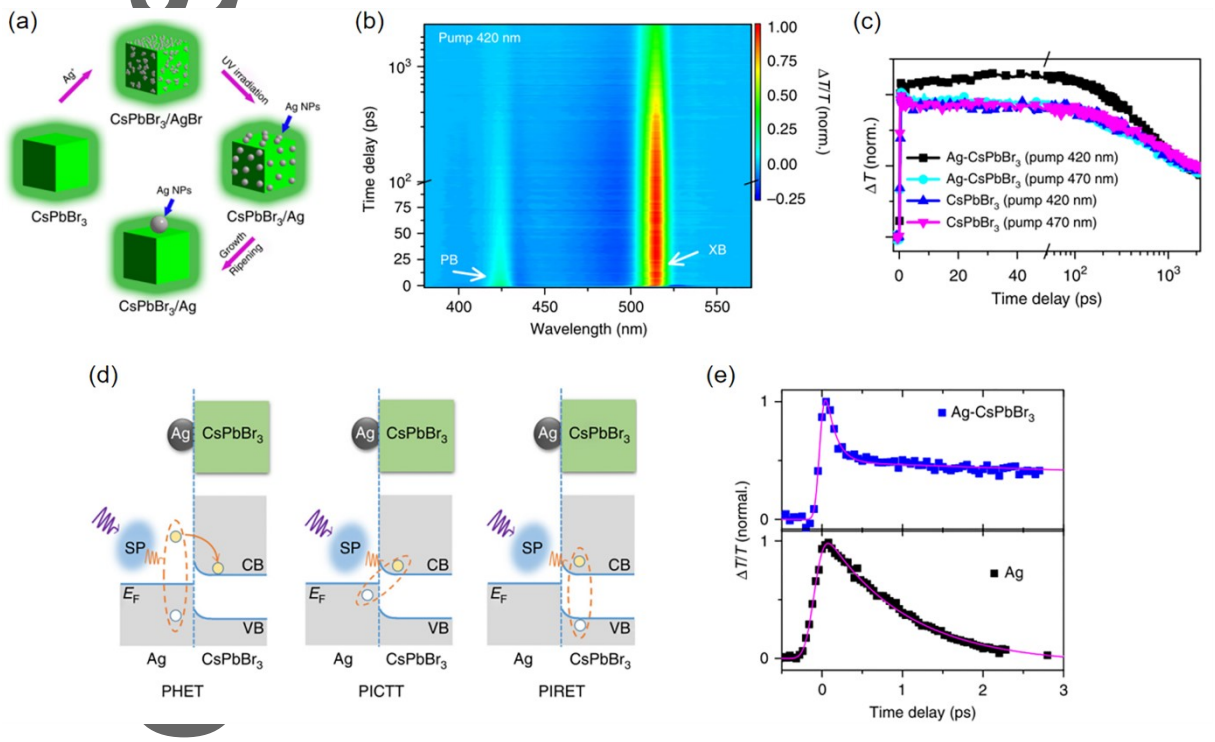

Figure 12. (a) Formation of Ag-$CsPbBr_3$ hybrid NCs. (b) TA data recorded from a solution sample of Ag-$CsPbBr_3$ NCs with a pump wavelength of 420 nm. In addition to the XB signal, an additional bleaching signal that is denoted as PB emerges at 424 nm, which was induced by the LSPR under resonant pump excitation. (c) Kinetic curves probed at 514 nm recorded from $CsPbBr_3$ and Ag-$CsPbBr_3$ NCs under 420 nm resonant and 470 nm off-resonant pump, respectively. (d) Schematic of interfacial excitation transfer processes. (e) Recombination dynamics probed at the LSPR wavelength in the samples of neat Ag nanoparticles and hybrid Ag-$CsPbBr_3$ NCs. Reproduced with permission.[56] Copyright 2019, Springer Nature.

5. Summary and perspective

This review focused on the characterization of the CT process in $CsPbX_3$ PeNCs by using the ultrafast TA technique. The key factors that reliable TA measurements require were intensively discussed involving the type of outer acceptors, the donor to acceptor ratio, the link between each, and the band alignment. We first presented a thorough interpretation of TA spectral features in association of the CT dynamics. Some concerns were discussed relating to the interpretation of the TA data acquired from PeNCs samples. The multiple CT pathways may lead to misestimation of CT rates especially in comparison to different PeNC systems. We suggest the use of the intrinsic CT rate in order to secure the rigor of TA measurements of CT dynamics. The ligands also play a crucial role in the CT process. The various causal factors such as the length of the ligand molecules, dipole moments and conductivity provide ways of modulating the CT process towards maximizing the efficiency of charge carrier extraction. However, these interlaced factors may complicate the interpretation of observed CT rates. Finally, we addressed recent work on hot carrier extraction which may boost the development of hot-carrier based solar cells that show potential for achieving over-SQ-limit photovoltaic technologies. We look forward to more extensive investigations in hot carrier extraction processes and this is one of our motivations of this review: TA provides the ability to reveal the ultrafast hot carrier dynamics while $CsPbX_3$ PeNCs are potential hot carrier materials possessing desirable properties such as long hot carrier relaxing time. We also highlighted studies on the exploration of plasmon-hot electron conversion pathways in $CsPbX_3$ PeNC-noble metal heterostructures, which is of great interest for hot carrier energy transfer. In addition, we compiled a table summarizing measurements of CT rates in various $CsPbX_3$ PeNCs complexes.

Obtaining accurate and reliable CT dynamics leads the way linking the fundamental mechanisms and practical applications for these novel nanostructures. The concerns addressed here are in fact among the most crucial issues in CT rates or efficiency characterization for most works. We expect that our discussion may help to regulate investigations of CT processes in the PeNC community using ultrafast spectroscopy techniques.

Acknowledgements

X.L., P.Z. and M.L. acknowledge support by National Key Research and Development Program of China (2017YFA0207400), National Natural Science Foundation of China (61905037 and 62104027). T.A.S. acknowledges support by the Australian Research Council Centre of Excellence in Exciton Science (CE170100026).

Conflict of Interest

The authors declare no conflict of interest.

Reference

[1] L. Protesescu, S. Yakunin, M. I. Bodnarchuk, F. Krieg, R. Caputo, C. H. Hendon, R. X. Yang, A. Walsh and M. V. Kovalenko, *Nano Lett.* **2015**, *15*, 3692.

[2] M. M. Lee, J. Teuscher, T. Miyasaka, T. N. Murakami and H. J. Snaith, *Science* **2012**, *338*, 643.

[3] J. Jeong, M. Kim, J. Seo, H. Lu, P. Ahlawat, A. Mishra, Y. Yang, M. A. Hope, F. T. Eickemeyer, M. Kim, Y. J. Yoon, I. W. Choi, B. P. Darwich, S. J. Choi, Y. Jo, J. H. Lee, B. Walker, S. M. Zakeeruddin, L. Emsley, U. Rothlisberger, A. Hagfeldt, D. S. Kim, M. Gratzel and J. Y. Kim, *Nature* **2021**, *592*, 381.

[4] J. Song, J. Li, X. Li, L. Xu, Y. Dong and H. Zeng, *Adv. Mater.* **2015**, *27*, 7162.

[5] H. Huang, L. Polavarapu, J. A. Sichert, A. S. Susha, A. S. Urban and A. L. Rogach, *NPG Asia Mater.* **2016**, *8*, e328.

[6] P. Ramasamy, D.-H. Lim, B. Kim, S.-H. Lee, M.-S. Lee and J.-S. Lee, *Chem. Commun.* **2016**, *52*, 2067.

[7] Y. Wang, X. Li, X. Zhao, L. Xiao, H. Zeng and H. Sun, *Nano Lett.* **2016**, *16*, 448.

[8] Q. Zhang and Y. Yin, *ACS Cent. Sci.* **2018**, *4*, 668.

[9] A. Pan, B. He, X. Fan, Z. Liu, J. J. Urban, A. P. Alivisatos, L. He and Y. Liu, *ACS Nano* **2016**, *10*, 7943.

[10] S. Sun, D. Yuan, Y. Xu, A. Wang and Z. Deng, *ACS Nano* **2016**, *10*, 3648.

[11] G. Almeida, L. Goldoni, Q. Akkerman, Z. Dang, A. H. Khan, S. Marras, I. Moreels and L. Manna, *ACS Nano* **2018**, *12*, 1704.

[12] X. Zhang, H. Lin, H. Huang, C. Reckmeier, Y. Zhang, W. C. H. Choy and A. L. Rogach, *Nano Lett.* **2016**, *16*, 1415.

[13] X. Zhang, C. Sun, Y. Zhang, H. Wu, C. Ji, Y. Chuai, P. Wang, S. Wen, C. Zhang and W. W. Yu, *J. Phys. Chem. Lett.* **2016**, *7*, 4602.

[14] J. Yuan, X. Ling, D. Yang, F. Li, S. Zhou, J. Shi, Y. Qian, J. Hu, Y. Sun, Y. Yang, X. Gao, S. Duhm, Q. Zhang and W. Ma, *Joule* **2018**, *2*, 2450.

[15] M. Gong, R. Sakidja, R. Goul, D. Ewing, M. Casper, A. Stramel, A. Elliot and J. Z. Wu, *ACS Nano* **2019**, *13*, 1772.

[16] G. R. Yettapu, D. Talukdar, S. Sarkar, A. Swarnkar, A. Nag, P. Ghosh and P. Mandal, *Nano Lett.* **2016**, *16*, 4838.

[17] R. Begum, M. R. Parida, A. L. Abdelhady, B. Murali, N. M. Alyami, G. H. Ahmed, M. N. Hedhili, O. M. Bakr and O. F. Mohammed, *J. Am. Chem. Soc.* **2017**, *139*, 731.

[18] N. Mondal and A. Samanta, *Nanoscale* **2017**, *9*, 1878.

[19] Y.-H. Kim, S. Kim, A. Kakekhani, J. Park, J. Park, Y.-H. Lee, H. Xu, S. Nagane, R. B. Wexler, D.-H. Kim, S. H. Jo, L. Martinez-Sarti, P. Tan, A. Sadhanala, G.-S. Park, Y.-W. Kim, B. Hu, H. J. Bolink, S. Yoo, R. H. Friend, A. M. Rappe and T.-W. Lee, *Nat. Photonics* **2021**, *15*, 148.

[20] C. Ruckebusch, M. Sliwa, P. Pernot, A. de Juan and R. Tauler, *J. Photochem. Photobiol., C* **2012**, *13*, 1.

[21] R. Berera, R. van Grondelle and J. T. Kennis, *Photosynth. Res.* **2009**, *101*, 105.

[22] J. Butkus, P. Vashishtha, K. Chen, J. K. Gallaher, S. K. K. Prasad, D. Z. Metin, G. Laufersky, N. Gaston, J. E. Halpert and J. M. Hodgkiss, *Chem. Mater.* **2017**, *29*, 3644.

[23] C. C. Qin, Z. N. Jiang, Z. P. Zhou, Y. F. Liu and Y. H. Jiang, *Nanomaterials-Basel* **2021**, *11*, 463.
[24] J. S. Manser and P. V. Kamat, *Nat. Photonics* **2014**, *8*, 737.
[25] N. Mondal, A. De, S. Das, S. Paul and A. Samanta, *Nanoscale* **2019**, *11*, 9796.
[26] D. W. deQuilettes, K. Frohna, D. Emin, T. Kirchartz, V. Bulovic, D. S. Ginger and S. D. Stranks, *Chem. Rev.* **2019**, *119*, 11007.
[27] D. Rossi, H. Wang, Y. T. Dong, T. Qiao, X. F. Qian and D. H. Son, *ACS Nano* **2018**, *12*, 12436.
[28] G. Ghosh, B. Jana, S. Sain, A. Ghosh and A. Patra, *Phys. Chem. Chem. Phys.* **2019**, *21*, 19318.
[29] G. Yumoto, H. Tahara, T. Kawawaki, M. Saruyama, R. Sato, T. Teranishi and Y. Kanemitsu, *J. Phys. Chem. Lett.* **2018**, *9*, 2222.
[30] G. Giorgi, J. Fujisawa, H. Segawa and K. Yamashita, *J. Phys. Chem. Lett.* **2013**, *4*, 4213.
[31] A. Amat, E. Mosconi, E. Ronca, C. Quarti, P. Umari, M. K. Nazeeruddin, M. Gratzel and F. De Angelis, *Nano Lett.* **2014**, *14*, 3608.
[32] J. Aneesh, A. Swarnkar, V. Kumar Ravi, R. Sharma, A. Nag and K. V. Adarsh, *J. Phys. Chem. C* **2017**, *121*, 4734.
[33] K. Wu, G. Liang, Q. Shang, Y. Ren, D. Kong and T. Lian, *J. Am. Chem. Soc.* **2015**, *137*, 12792.
[34] F. Liu, Y. Zhang, C. Ding, T. Toyoda, Y. Ogomi, T. S. Ripolles, S. Hayase, T. Minemoto, K. Yoshino, S. Dai and Q. Shen, *J. Phys. Chem. Lett.* **2018**, *9*, 294.
[35] N. Monday, A. De and A. Samanta, *J. Phys. Chem. Lett.* **2018**, *9*, 3673.
[36] J. Wang, T. Ding, J. Leng, S. Jin and K. Wu, *J. Phys. Chem. Lett.* **2018**, *9*, 3372.
[37] P. Maity, J. Dana and H. N. Ghosh, *J. Phys. Chem. C* **2016**, *120*, 18348.
[38] S. Mandal, L. George and N. V. Tkachenko, *Nanoscale* **2019**, *11*, 862.
[39] H. Zhu, Y. Yang, K. Hyeon-Deuk, M. Califano, N. Song, Y. Wang, W. Zhang, O. V. Prezhdo and T. Lian, *Nano Lett.* **2014**, *14*, 1263.
[40] E. J. Piechota and G. J. Meyer, *J. Chem. Educ.* **2019**, *96*, 2450.
[41] J. H. Olshansky, T. X. Ding, Y. V. Lee, S. R. Leone and A. P. Alivisatos, *J. Am. Chem. Soc.* **2015**, *137*, 15567.
[42] A. Brumberg, B. T. Diroll, G. Nedelcu, M. E. Sykes, Y. Liu, S. M. Harvey, M. R. Wasielewski, M. V. Kovalenko and R. D. Schaller, *Nano Lett.* **2018**, *18*, 4771.
[43] G. H. Ahmed, J. K. Liu, M. R. Parida, B. Murali, R. Bose, N. M. AlYami, M. N. Hedhili, W. Peng, J. Pan, T. M. D. Besong, O. M. Bakr and O. F. Mohammed, *J. Phys. Chem. Lett.* **2016**, *7*, 3913.
[44] A. De, N. Mondal and A. Samanta, *J. Phys. Chem. C* **2018**, *122*, 13617.
[45] J. Dai, J. Xi, L. Li, J. Zhao, Y. Shi, W. Zhang, C. Ran, B. Jiao, X. Hou, X. Duan and Z. Wu, *Angew. Chem., Int. Ed. Engl.* **2018**, *57*, 5754.
[46] J. Dana, P. Maity, B. Jana, S. Maiti and H. N. Ghosh, *ACS Omega* **2018**, *3*, 2706.
[47] M. Li, S. Bhaumik, T. W. Goh, M. S. Kumar, N. Yantara, M. Gratzel, S. Mhaisalkar, N. Mathews and T. C. Sum, *Nat. Commun.* **2017**, *8*, 14350.
[48] P. Zhang, G. Zhu, Y. Shi, Y. Wang, J. Zhang, L. Du and D. Ding, *J. Phys. Chem. C* **2018**, *122*, 27148.
[49] R. A. Scheidt, E. Kerns and P. V. Kamat, *J. Phys. Chem. Lett.* **2018**, *9*, 5962.

[50] B. J. Roman, J. Otto, C. Galik, R. Downing and M. Sheldon, *Nano Lett.* **2017**, *17*, 5561.
[51] A. Pan, X. Ma, S. Huang, Y. Wu, M. Jia, Y. Shi, Y. Liu, P. Wangyang, L. He and Y. Liu, *J. Phys. Chem. Lett.* **2019**, *10*, 6590.
[52] E. Rathore, K. Maji, D. Rao, B. Saha and K. Biswas, *J. Phys. Chem. Lett.* **2020**, *11*, 8002.
[53] J. Yun, H. Fan, Y. Zhang, R. Huang, Y. Ren, M. Guo, H. An, P. Kang and H. Guo, *ACS Appl. Mater. Interfaces* **2020**, *12*, 3086.
[54] M. Imran, L. Peng, A. Pianetti, V. Pinchetti, J. Ramade, J. Zito, F. Di Stasio, J. Buha, S. Toso, J. Song, I. Infante, S. Bals, S. Brovelli and L. Manna, *J. Am. Chem. Soc.* **2021**, *143*, 1435.
[55] J. Chakkamalayath, G. V. Hartland and P. V. Kamat, *J. Phys. Chem. C* **2021**, *125*, 17881.
[56] X. Huang, H. Li, C. Zhang, S. Tan, Z. Chen, L. Chen, Z. Lu, X. Wang and M. Xiao, *Nat. Commun.* **2019**, *10*, 1163.
[57] Y. X. Zhang, H. Y. Wang, Z. Y. Zhang, Y. Zhang, C. Sun, Y. Y. Yue, L. Wang, Q. D. Chen and H. B. Sun, *Phys. Chem. Chem. Phys.* **2017**, *19*, 1920.
[58] N. H. Song, H. M. Zhu, S. Y. Jin, W. Zhan and T. Q. Lian, *ACS Nano* **2011**, *5*, 613.
[59] M. Li, S. R. Valandro, R. He, Y. Zhao, P. Yang and K. S. Schanze, *J. Phys. Chem. C* **2021**, *125*, 14778.
[60] Q. Shang, A. L. Kaledin, Q. Li and T. Lian, *J. Chem. Phys.* **2019**, *151*, 074705.
[61] A. J. Morris-Cohen, M. T. Frederick, L. C. Cass and E. A. Weiss, *J. Am. Chem. Soc.* **2011**, *133*, 10146.
[62] S. Sarkar, V. K. Ravi, S. Banerjee, G. R. Yettapu, G. B. Markad, A. Nag and P. Mandal, *Nano Lett.* **2017**, *17*, 5402.
[63] J. De Roo, M. Ibanez, P. Geiregat, G. Nedelcu, W. Walravens, J. Maes, J. C. Martins, I. Van Driessche, M. V. Kovalenko and Z. Hens, *ACS Nano* **2016**, *10*, 2071.
[64] S. Mandal and N. V. Tkachenko, *J. Phys. Chem. Lett.* **2019**, *10*, 2775.
[65] X. Luo, G. Liang, J. Wang, X. Liu and K. Wu, *Chem. Sci.* **2019**, *10*, 2459.
[66] Q. Shang, B. D. Piercy, M. D. Losego and T. Lian, *J. Phys. Chem. C* **2019**, *123*, 21415.
[67] W. Zheng, Q. Wan, M. Liu, Q. Zhang, C. Zhang, R. Yan, X. Feng, L. Kong and L. Li, *J. Phys. Chem. C* **2021**, *125*, 3110.
[68] J. Kim, L. Hu, H. Chen, X. Guan, P. R. Anandan, F. Li, J. Tang, C.-H. Lin, K. Kalantar-Zadeh, A. Tricoli and T. Wu, *ACS Mater. Lett.* **2020**, *2*, 1368.
[69] J. H. Li, L. M. Xu, T. Wang, J. Z. Song, J. W. Chen, J. Xue, Y. H. Dong, B. Cai, Q. S. Shan, B. N. Han and H. B. Zeng, *Adv. Mater.* **2017**, *29*, 1603885.
[70] Y. Tezuka, K. Umemoto, M. Takeda, Y. Takahashi, H. Ebe, J. Enomoto, S. Rodbuntum, T. Nohara, D. Fontecha, S. Asakura, T. Chiba, M. I. Furis, T. Yoshida, H. Uji-i and A. Masuhara, *Jpn. J. Appl. Phys.* **2020**, *59*, SDDC04.
[71] E. T. Vickers, K. Xu, X. Li and J. Z. Zhang, *J. Chem. Phys.* **2020**, *152*, 034701.
[72] E. T. Vickers, T. A. Graham, A. H. Chowdhury, B. Bahrami, B. W. Dreskin, S. Lindley, S. B. Naghadeh, Q. Qiao and J. Z. Zhang, *ACS Energy Lett.* **2018**, *3*, 2931.
[73] G. Li, J. Huang, H. Zhu, Y. Li, J.-X. Tang and Y. Jiang, *Chem. Mater.* **2018**, *30*, 6099.
[74] S. Dey, H. Cohen, I. Pinkas, H. Lin, M. Kazes and D. Oron, *J. Chem. Phys.* **2019**, *151*, 174704.
[75] X. Liu, H. Zhao, L. Wei, X. Ren, X. Zhang, F. Li, P. Zeng and M. Liu, *Nanophotonics* **2021**, *10*, 1967.

[76] Y. Gong, J. Shen, Y. Zhu, W. Yan, J. Zhu, L. Hou, D. Xie and C. Li, *Appl. Surf. Sci.* **2021**, *545*, 149012.
[77] A. Loiudice, S. Saris and R. Buonsanti, *J. Phys. Chem. Lett.* **2020**, *11*, 3430.
[78] A. Kipkorir, J. DuBose, J. Cho and P. V. Kamat, *Chem. Sci.* **2021**, *12*, 14815.
[79] Z. X. Yin, J. Leng, S. P. Wang, G. J. Liang, W. M. Tian, K. F. Wu and S. Y. Jin, *J. Am. Chem. Soc.* **2021**, *143*, 4725.
[80] M. C. Gelvez-Rueda, M. B. Fridriksson, R. K. Dubey, W. F. Jager, W. van der Stam and F. C. Grozema, *Nat. Commun.* **2020**, *11*, 1901.
[81] K. Marjit, G. Ghosh, S. Ghosh, S. Sain, A. Ghosh and A. Patra, *J. Phys. Chem. C* **2021**, *125*, 12214.
[82] Q. Y. Li and T. Q. Lian, *J. Phys. Chem. Lett.* **2019**, *10*, 566.
[83] K. B. Zheng, Y. N. Chen, Y. Sun, J. S. Chen, P. Chabera, R. Schaller, M. J. Al-Marri, S. E. Canton, Z. Q. Liang and T. Pullerits, *J. Mater. Chem. A* **2018**, *6*, 6244.
[84] S. M. Kobosko, J. T. DuBose and P. V. Kamat, *ACS Energy Lett.* **2019**, *5*, 221.
[85] J. T. DuBose and P. V. Kamat, *J. Phys. Chem. C* **2020**, *124*, 12990.
[86] E. P. Yao, B. J. Bohn, Y. Tong, H. Huang, L. Polavarapu and J. Feldmann, *Adv. Opt. Mater.* **2019**, *7*, 1801776.
[87] G. Ghosh, K. Marjit, S. Ghosh, A. Ghosh, R. Ahammed, A. De Sarkar and A. Patra, *J. Phys. Chem. C* **2021**, *125*, 5859.
[88] A. De, S. Das and A. Samanta, *ACS Energy Lett.* **2020**, *5*, 2246.
[89] J. F. Liao, Y. F. Xu, X. D. Wang, H. Y. Chen and D. B. Kuang, *ACS Appl. Mater. Interfaces* **2018**, *10*, 42301.
[90] J. T. DuBose and P. V. Kamat, *J. Phys. Chem. Lett.* **2019**, *10*, 6074.
[91] J.-F. Liao, Y.-T. Cai, J.-Y. Li, Y. Jiang, X.-D. Wang, H.-Y. Chen and D.-B. Kuang, *J. Energy Chem.* **2021**, *53*, 309.
[92] W. Shockley and H. J. Queisser, *J. Appl. Phys.* **1961**, *32*, 510.
[93] R. T. Ross and A. J. Nozik, *J. Appl. Phys.* **1982**, *53*, 3813.
[94] M. A. Green, *Prog. Photovolt: Res. Appl.* **2001**, *9*, 123.
[95] Z. Guo, Y. Wan, M. Yang, J. Snaider, K. Zhu and L. Huang, *Science* **2017**, *356*, 59.
[96] J. Sung, S. Macpherson and A. Rao, *J. Phys. Chem. Lett.* **2020**, *11*, 5402.
[97] J. Y. Sung, C. Schnedermann, L. M. Ni, A. Sadhanala, R. Y. S. Chen, C. Cho, L. Priest, J. M. Lim, H. K. Kim, B. Monserrat, P. Kukura and A. H. Rao, *Nat. Phys.* **2020**, *16*, 171.
[98] S. S. Lim, D. Giovanni, Q. N. Zhang, A. Solanki, N. F. Jamaludin, J. W. M. Lim, N. Mathews, S. Mhaisalkar, M. S. Pshenichnikov and T. C. Sum, *Sci. Adv.* **2019**, *5*, eaax3620.
[99] G. Xing, N. Mathews, S. Sun, S. Lim Swee, M. Lam Yeng, M. Grätzel, S. Mhaisalkar and C. Sum Tze, *Science* **2013**, *342*, 344.
[100] S. Kaniyankandy and S. Neogy, *J. Photochem. Photobiol., A* **2020**, *401*, 112761.
[101] T. R. Hopper, A. Gorodetsky, A. Jeong, F. Krieg, M. I. Bodnarchuk, M. Maimaris, M. Chaplain, T. J. Macdonald, X. Huang, R. Lovrincic, M. V. Kovalenko and A. A. Bakulin, *Nano Lett.* **2020**, *20*, 2271.
[102] J. W. M. Lim, D. Giovanni, M. Righetto, M. Feng, S. G. Mhaisalkar, N. Mathews and T. C. Sum, *J. Phys. Chem. Lett.* **2020**, *11*, 2743.
[103] M. Cong, B. Yang, J. Chen, F. Hong, S. Yang, W. Deng and K. Han, *J. Phys. Chem. Lett.* **2020**, *11*, 1921.

[104] M. E. Madjet, G. R. Berdiyorov, F. El-Mellouhi, F. H. Alharbi, A. V. Akimov and S. Kais, *J. Phys. Chem. Lett.* **2017**, *8*, 4439.
[105] H. Chung, S. I. Jung, H. J. Kim, W. Cha, E. Sim, D. Kim, W. K. Koh and J. Kim, *Angew. Chem. Int. Ed. Engl.* **2017**, *56*, 4160.
[106] T. R. Hopper, A. Gorodetsky, J. M. Frost, C. Muller, R. Lovrincic and A. A. Bakulin, *ACS Energy Lett* **2018**, *3*, 2199.
[107] J. Fu, Q. Xu, G. Han, B. Wu, C. H. A. Huan, M. L. Leek and T. C. Sum, *Nat. Commun.* **2017**, *8*, 1300.
[108] Y. Yang, D. P. Ostrowski, R. M. France, K. Zhu, J. van de Lagemaat, J. M. Luther and M. C. Beard, *Nat. Photonics* **2016**, *10*, 53.
[109] Z. H. Nie, X. Z. Gao, Y. J. Ren, S. Y. Xia, Y. H. Wang, Y. L. Shi, J. Zhao and Y. Wang, *Nano Lett.* **2020**, *20*, 4610.
[110] G. Kaur, K. J. Babu, N. Ghorai, T. Goswami, S. Maiti and H. N. Ghosh, *J. Phys. Chem. Lett.* **2019**, *10*, 5302.
[111] J. F. Yang, X. M. Wen, H. Z. Xia, R. Sheng, Q. S. Ma, J. Kim, P. Tapping, T. Harada, T. W. Kee, F. Z. Huang, Y. B. Cheng, M. Green, A. Ho-Baillie, S. J. Huang, S. Shrestha, R. Patterson and G. Conibeer, *Nat. Commun.* **2017**, *8*, 14120.
[112] J. S. Chen, M. E. Messing, K. B. Zheng and T. Pullerits, *J. Am. Chem. Soc.* **2019**, *141*, 3532.
[113] K. Marjit, G. Ghosh, R. K. Biswas, S. Ghosh, S. K. Pati and A. Patra, *J. Phys. Chem. Lett.* **2022**, *13*, 5431.
[114] Q. Wei, J. Yin, O. M. Bakr, Z. Wang, C. H. Wang, O. F. Mohammed, M. J. Li and G. C. Xing, *Angew. Chem., Int. Ed. Engl.* **2021**, *60*, 10957.
[115] J. Meng, Z. Y. Lan, W. H. Lin, M. L. Liang, X. S. Zou, Q. Zhao, H. F. Geng, I. E. Castelli, S. E. Canton, T. Pullerits and K. B. Zheng, *Chem. Sci.* **2022**, *13*, 1734.
[116] G. Ghosh, R. K. Biswas, K. Marjit, S. Ghosh, A. Ghosh, S. K. Pati and A. Patra, *Adv. Opt. Mater.* **2022**, *10*, 2200030.
[117] P. Zeng, X. Ren, L. Wei, H. Zhao, X. Liu, X. Zhang, Y. Xu, L. Yan, K. Boldt, T. A. Smith and M. Liu, *Angew. Chem., Int. Ed. Engl.* **2022**, *61*, e202111443.
[118] G. Kaur, R. Saha, K. J. Babu, A. Shukla and H. N. Ghosh, *J. Phys. Chem. C* **2021**, *125*, 10516.
[119] J. A. Schuller, E. S. Barnard, W. Cai, Y. C. Jun, J. S. White and M. L. Brongersma, *Nat. Mater.* **2010**, *9*, 193.
[120] C. Clavero, *Nat. Photonics* **2014**, *8*, 95.

Xiaochun Liu received her bachelor and Ph.D. degree at Jilin University in China. She is currently working as a postdoc at University of Electronic Science and Technology of China. She worked on ultrafast transient absorption spectroscopy under a variety of measuring conditions including ultrahigh pressure and cryogenic environment. After joining Prof. Mingzhen Liu's group in 2019, Dr. X. Liu started researches covering ultrafast photocarrier dynamics of all inorganic perovskite nanocrystals and theoretical chemical dynamics. She also works on development of ultrafast spectroscopy techniques including broadband fluorescence up-conversion and transient grating spectroscopy.

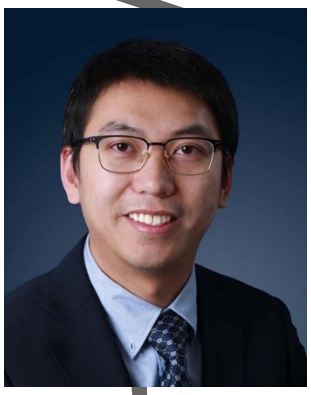

Peng Zeng completed his undergraduate at Tsinghua University and Ph.D. courses under supervision of Prof. T. A. Smith at University of Melbourne, respectively. He joint University of Electronic Science and Technology of China as an associate professor in 2018. Before joining UESTC, Dr. P. Zeng studied photo-induced ultrafast charge transfer processes of diverse nanostructures by ultrafast optical spectroscopy. His current research interest covers both fundamental theories and applications of novel optoelectronic materials, with a focus on photocarrier dynamics through combination of simulation and ultrafast time-resolved spectroscopy.

Trevor A. Smith obtained his BSc (Hons) and PhD degrees from the University of Melbourne before being awarded an Australian National Teaching Company Scheme Scholarship. He then completed a post-doctoral position at Imperial College, London before returning to the University of Melbourne as an Ernst & Grace Matthaei Research Fellow and was subsequently awarded an Australian Research Council (ARC) QEII Fellowship. He leads the Ultrafast and Microspectroscopy Laboratories in the School of Chemistry at the University or Melbourne and is a Chief Investigator in the ARC Centre of Excellence in Exciton Science.

Mingzhen Liu received her undergraduate degree at University of Bristol and pursued her M.Phil. at University of Cambridge. Later she got her Ph.D. degree at University of Oxford. In 2016, she joined University of Electronic Science and Technology of China. Her research focuses on perovskite materials and related photonic and optoelectronic devices, and now leads a synthesis group for perovskite-based optoelectronics materials and devices at UESTC. Besides PeNC-related fundamental research and applications, the group so far has achieved exciting outputs including high-efficiency perovskite photovoltaic deceives and photodetectors.

This review provides a summary of recent research works on characterization of the CT process in $CsPbX_3$ PeNCs by using the ultrafast TA technique, in an attempt to address the concerns of multiple CT pathway effects, surface ligand effects and hot carrier extraction in CT characterization and thus to unravel the underlying mechanisms of the CT process in $CsPbX_3$ PeNCs.

Xiaochun Liu,[#] Peng Zeng,[#] Shuhan Chen, Trevor A. Smith, and Mingzhen Liu*

Charge Transfer Dynamics at the Interface of $CsPbX_3$ Perovskite Nanocrystal-Acceptor Complexes: a Femtosecond Transient Absorption Spectroscopy Study